EFFECTS OF A SINGLE MAGNETIC IMPURITY ON SUPERCONDUCTIVITY

A Thesis Submitted to the

College of Graduate Studies and Research

in Partial Fulfillment of the Requirements

for the degree of Master of Science

in the Department of Physics and Engineering Physics

University of Saskatchewan

Saskatoon

By

Sushan Pan

Permission to Use

In presenting this thesis in partial fulfilment of the requirements for a Postgraduate degree from the University of Saskatchewan, I agree that the Libraries of this University may make it freely available for inspection. I further agree that permission for copying of this thesis in any manner, in whole or in part, for scholarly purposes may be granted by the professor or professors who supervised my thesis work or, in their absence, by the Head of the Department or the Dean of the College in which my thesis work was done. It is understood that any copying or publication or use of this thesis or parts thereof for financial gain shall not be allowed without my written permission. It is also understood that due recognition shall be given to me and to the University of Saskatchewan in any scholarly use which may be made of any material in my thesis.

Requests for permission to copy or to make other use of material in this thesis in whole or part should be addressed to:

Head of Department of Physics and Engineering Physics
116 Science Place
University of Saskatchewan
Saskatoon, Saskatchewan
Canada
S7N 5E2

Abstract

Electronic structure of a conventional superconductor in the vicinity of a single, isolated magnetic impurity has been probed experimentally with scanning tunneling spectroscopy by Yazdani *et al.*. Motivated by their experiment, we study the effects of a single magnetic impurity on superconductivity by means of the mean-field Bogoliubov-de Gennes theory. The Bogoliubov-de Gennes equations are solved directly and numerically, utilizing parallel computation on a CFI-founded 128-CPU Beowulf-class PC cluster here at the University of Saskatchewan. As a preliminary study, we also examine the electronic structure around a magnetic vortex. The local magnetic field around a vortex breaks up Cooper pairs and suppresses superconductivity locally. Quasiparticle excitations are created and bound in the vortex core area due to repeated Andreev scattering. A magnetic impurity tends to align the spins of the neighboring electrons and break up Cooper pairs, and has similar effects of locally suppressing superconductivity. A striking difference, however, from the vortex problem is that around a magnetic impurity there is particle-hole asymmetry in the tunneling conductance. This is due to different probability amplitudes in the spin-up branch and the spin-down branch of quasiparticle excitations. Furthermore, for the spin potential strength larger than a certain critical value, the nature of quasiparticle excitations is changed dramatically. Within a model of classical spin, we propose an explanation of the measured tunneling conductance of the experiment. This work is significant in that it gives us insight into superconductivity and magnetism–two complementary manifestation of strong electron correlations.

Acknowledgements

I would like to thank my supervisor, Dr. Kaori Tanaka, for her guidance and support throughout this project. I would also like to thank my committee members, Drs. Gap Soo Chang, Rainer Dick and Glenn Hussey, and the external examiner Dr. Chris Soteros for helpful comments and discussions. Financial support by the Natural Sciences and Engineering Research Council of Canada is gratefully acknowledged. I am also grateful to the support staff of the Department of Physics and Engineering Physics.

This thesis is dedicated to my parents, Pan and Hong

Contents

List of Figures

List of Abbreviations

T_c	critical temperature
H_c	critical magnetic field
STM	scanning tunneling microscope
STS	scanning tunneling spectroscopy
LDOS	local density of states
DOS	density of states
BdG	the Bogoliubov-de Gennes theory
BCS	the Bardeen-Cooper-Schrieffer theory
CdM	Caroli, de Gennes, and Matricon
GS	Gygi and Schlüter
GL	the Ginzburg-Landau theory
MPI	message passing interface

Chapter 1

Introduction

1.1 Motivation

1.1.1 Magnetic Properties of Superconductors

Superconductivity is a phenomenon first discovered by Kamerlingh Onnes in 1911 [1]. In his experiment, he found that electrical resistivity of mercury dropped sharply to zero when temperature T was decreased below a critical value T_c (4 K for mercury). This property of a superconductor holds if the magnitude of the electrical current is smaller than a critical value J_c. In addition to this perfect conductivity, a key feature that distinguishes a superconductor from a perfect conductor is perfect diamagnetism, the so-called Meissner effect discovered by Meissner and Ochsenfeld in 1933 [2]. Both a perfect conductor and a superconductor exclude magnetic field. However, when magnetic field is applied before cooling down, perfect conductivity and superconductivity show different properties. While a perfect conductor keeps trapping the field, a superconductor *expels* the magnetic field for $T < T_c$. Diamagnetism in the interior of the superconductor is maintained by supercurrent on the surface. The thickness of the region where the supercurrent exists and magnetic field is nonzero, is called the penetration depth, denoted by λ. This distinct property of a superconductor is lost for the field strength larger than a critical value H_c. At H_c, the magnitude of supercurrent exceeds J_c and thus the material can no longer maintain superconductivity.

In 1957, Bardeen, Cooper and Schrieffer proposed a microscopic theory, the so-called Bardeen-Cooper-Schrieffer (BCS) theory [3, 4, 5], which has successfully ex-

plained many properties of superconductors. According to the BCS theory, in the ground state (at absolute zero temperature) of a superconductor, two electrons of opposite momenta and spins $\vec{k}\uparrow$ and $-\vec{k}\downarrow$ form the so-called Cooper pair, through the exchange of phonons. The BCS theory is based on mean-field theory for the electron-phonon interaction. A typical distance between the two electrons of a Cooper pair is called the coherence length, denoted by ξ. In the ground state, all the electrons participate in the pairing, and all the Cooper pairs collectively form a macroscopic condensate due to strong correlation among the Cooper pairs. This is the origin of zero resistivity and "stiffness" against magnetic field of a superconductor. One needs a certain amount of energy, called energy gap, to break a Cooper pair. At finite temperature or under small external perturbation, some Cooper pairs are broken up, and the so-called quasiparticles are created, which are superposition of an electron and a hole. This "two fluid" picture describes conventional superconductivity very well. Although the BCS theory is limited for weak electron-phonon coupling and for homogeneous systems, it provides the fundamental understanding of superconductivity.

Since the first discovery of superconductivity at 4 K, the quest for new superconducting materials has led to a slow increase in known T_c over the decades. Finally the highest T_c seemed to have reached a plateau in Nb_3Ge (T_c=23 K) [6]. Thus the discovery of superconductivity at $T_c \approx 35$ K of "LBCO" in 1986 (a mixed oxide of lanthanum, barium, and copper) by Bednorz and Müller [7] came as a big surprise. Another big jump to $T_c \approx 90$ K in the "YBCO" class of materials followed immediately, and yet higher T_c values have been achieved in the "BSCCO" and "TBCCO" systems. These so-called high-temperature or unconventional superconductors are distinct from the "low-temperature" or "conventional" superconductors which can be well understood in terms of the BCS theory. The mechanism of high-T_c superconductivity is still not known. Furthermore, there are some properties of low-T_c superconductors that cannot be described by the "conventional" BCS theory. Thus extensive research in the area of superconductivity still continues today.

In the same year as the emergence of the BCS theory, in terms of the phenomeno-

logical Ginzburg-Landau (GL) theory, Abrikosov predicted that magnetic field can penetrate into the superconductor in the form of "vortices" [8], if $\lambda/\xi > 1/\sqrt{2}$. Around a vortex, superconductivity is suppressed in a region characterized by ξ, where quasiparticles are created and supercurrent flows, as shown in Fig. 1.1(a) [9]. A vortex is a magnetic flux carrying a flux quantum $\phi_0 = \frac{hc}{2e}$, where $2e$ is the charge

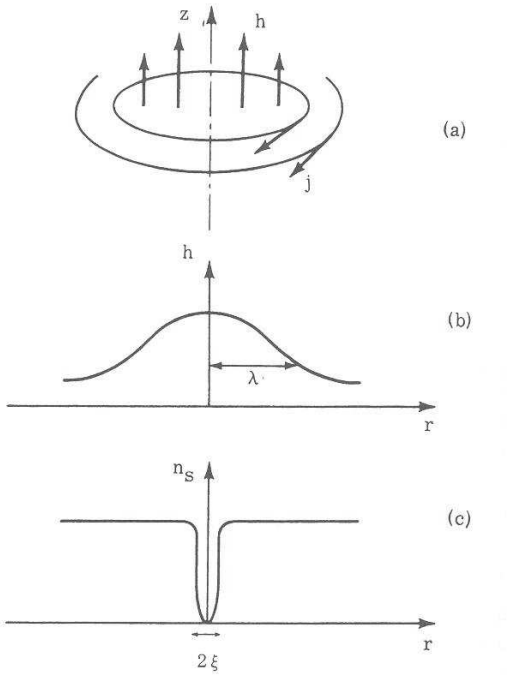

Figure 1.1: Illustration of the current j around a vortex creating local field h (a), penetration depth λ (b) and coherence length ξ (c). The n_s is the Cooper pair density [9].

of a Cooper pair,h is the Planck constant and c is the speed of light. Magnetic field decays over the length scale λ from the vortex center. The two length scales λ and ξ are illustrated in Fig. 1.1 (b) and (c), respectively. The number of vortices increases as the field is increased, and due to the magnetic interaction among vortices, they form a hexagonal lattice, called the Abrikosov vortex lattice [8]. The existence of such a vortex lattice was first observed ten years later by a magnetic decoration technique [10]. More recently, scanning tunneling spectroscopy (STS) measurements not only confirmed the existence of a vortex array, but also probed the local density of states (LDOS) of quasiparticles around a vortex [11, 12].

Superconductors with $\lambda/\xi > 1/\sqrt{2}$ which can sustain the vortex state are called

type-II superconductors, while those with $\lambda/\xi < 1/\sqrt{2}$ are called type-I. In a type-I superconductor, as the field is increased beyond H_c, the superconductor makes transition from the Meissner state to the normal state. Type-II superconductors have two critical fields H_{c1} and H_{c2}, which separate the Meissner phase from the vortex phase and the vortex phase from the normal phase, respectively. Some type-II superconductors have a third critical field H_{c3}, where for $H_{c2} < H < H_{c3}$, superconductivity remains on the surface of the material. The phase diagram of such a superconductor is illustrated in Fig. 1.2. Conventional superconductors are either type-I or type-II,

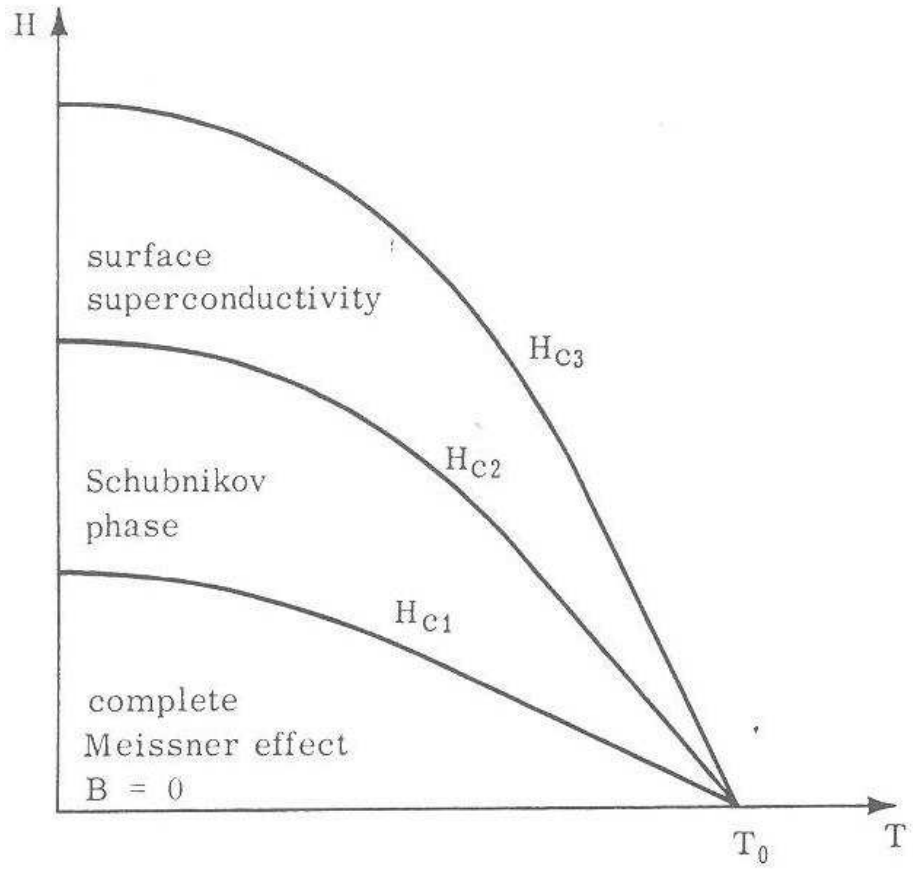

Figure 1.2: The field-temperature phase diagram of a type-II superconductor with three critical fields. Here $T_0 \equiv T_c$ is the zero-field transition temperature [9].

while most unconventional superconductors are type-II.

Even in conventional superconductors, vortices are complex objects and present intriguing properties. The magnetic field breaks up Cooper pairs and creates quasiparticle excitations around a vortex. Caroli, de Gennes, and Matricon (CdM) pre-

dicted the existence of quasiparticle bound states in the vortex core region [13, 14]. This was later confirmed by STS experiments on $NbSe_2$ [11, 12].

CdM discovered vortex bound states by means of semiclassical approximation to the Bogoliubov-de Gennes (BdG) equations, which will be introduced in Sec. 1.3.. The Bogoliubov-de Gennes (BdG) theory is a generalization of the BCS theory so that it can incorporate inhomogeneity due to magnetic field or impurities. It is a mean-field theory that is equivalent to the BCS theory for a homogeneous system with translational invariance. Almost 30 years after CdM, Gygi and Schlüter (GS) solved the BdG equations numerically and confirmed the existence of vortex bound states.

In this thesis, we first study electronic structure around a single vortex by solving the BdG equations selfconsistently. In this way, we can examine the pair-breaking effects of local magnetic field. Furthermore, by reproducing the results obtained by GS, we can make sure that our BdG program works properly. In this thesis, we choose to study inhomogeneity effects on conventional superconductivity. Its basic mechanism is well understood in terms of the BCS theory, and thus it is a good starting point. The best conventional superconductor for studying the vortex problem is $NbSe_2$ [15]. Single crystals of $NbSe_2$ can be easily made and are easy to cleave for creating a very clean surface that is ideal for STS. It is one of the few materials in which vortices have been observed clearly.

Like a magnetic vortex, a magnetic impurity also tends to break up Cooper pairs and suppress superconductivity locally. The main goal of this thesis is to understand the intriguing effects of a magnetic impurity on conventional superconductors and competition between superconductivity and magnetism.

Numerical codes are developed for a homogeneous system in two and three dimensions, the single vortex problem, and the problem of a magnetic impurity in a spherically symmetric system. Programs are parallelized utilizing Message Passing Interface (MPI).

1.1.2 Effects of a Magnetic Impurity

The Anderson theorem [16] states that nonmagnetic impurities do not reduce the critical temperature T_c in conventional isotropic superconductors. (An exception is the case for strong electron-phonon interaction and weak impurity potential [17].) A magnetic impurity, on the other hand, tends to align spins of nearby electrons with its own spin, break time-reversal symmetry and suppress superconductivity [18, 19].

Electronic structure of a conventional superconductor in the vicinity of a single, isolated magnetic impurity has been probed with scanning tunneling microscope (STM) by Yazdani *et al.* [20]. This experiment has motivated our research project. our aim is to examine electronic structure around a single magnetic atom in a conventional superconductor by means of the selfconsistent BdG theory. No selfconsistent calculation in the framework of the BdG theory to understand this experiment has been made so far. The BdG equations are solved directly and numerically. Numerical difficulties are overcame by utilizing parallel computation on a large-scale Beowulf-class PC cluster here at the University of Saskatchewan.

There were two parts in the experiment of Ref. [20]. First, the local tunneling conductance, dI/dV, was measured on a clean Nb sample. Second, two kinds of magnetic atom, Mn and Gd, and a nonmagnetic atom Ag were deposited separately on three pure Nb samples. Measurement of dI/dV was repeated around each of the three kinds of impurity atoms and far away from the atoms. By comparing the results, the effects of magnetic impurity were revealed.

The experimental method, STS, is an important surface analysis technique. This technique is based on quantum tunneling effect. When the sample surface is close enough to the metallic tip that is sharpened to a single atomic precision, and a voltage is applied between them, electrons can tunnel through the vacuum barrier, and thus currents flow between the tip and the sample. The tunneling conductance dI/dV is proportional to the product of the LDOS at the tip and the LDOS at the sample. The LDOS at the tip can be assumed to be a constant, and thus the tunneling conductance as a function of bias voltage can map out the LDOS as a

function of energy in the sample.

Figure 1.3(a) is the tunneling conductance of a pure Nb sample obtained in the experiment of Ref. [20]. One can see clearly an energy gap around zero bias voltage

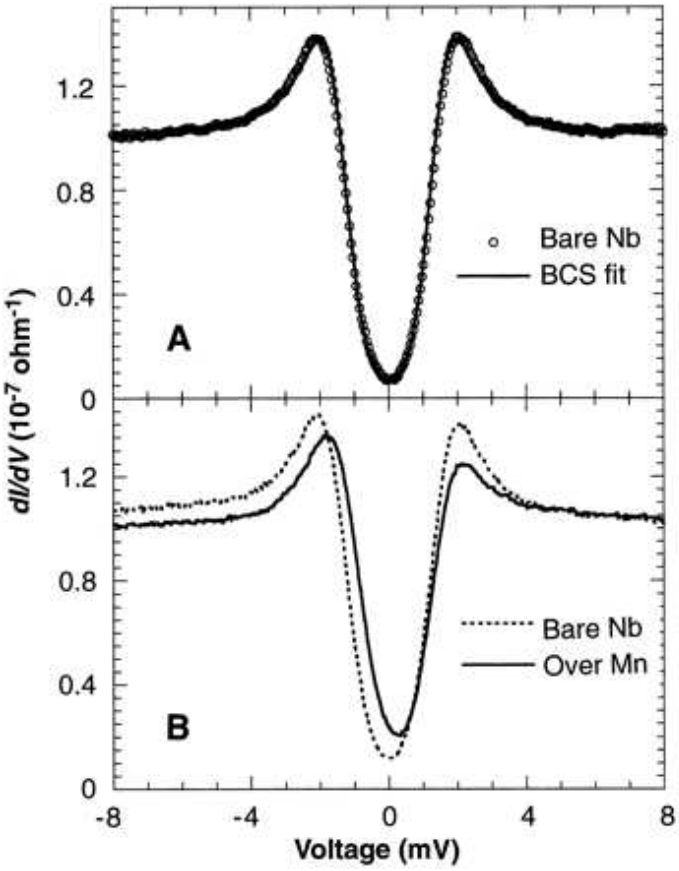

Figure 1.3: Tunneling conductance of the experiment of Ref.[20]; of a pure sample (A) and over a magnetic impurity (B).

and the so-called coherence peak (explained later) at the gap edge. The solid and dashed curves in Fig. 1.3(b) are the tunneling conductance measured around a single Mn atom and that measured far away from the impurity, respectively. The tunneling conductance obtained far away from the impurity is similar to that obtained on a pure sample. However, the tunneling conductance around the impurity atom shows that there are extra states inside the gap, and that it exhibits particle-hole asymmetry.

To see the effects of the impurities, the tunneling conductance difference (the bulk dI/dV measured at 30 Å away from the impurity atom subtracted from the tunneling conductance data) for the three samples with different impurity atoms

were measured as shown in Fig. 1.4. The difference spectra reflect the effects of

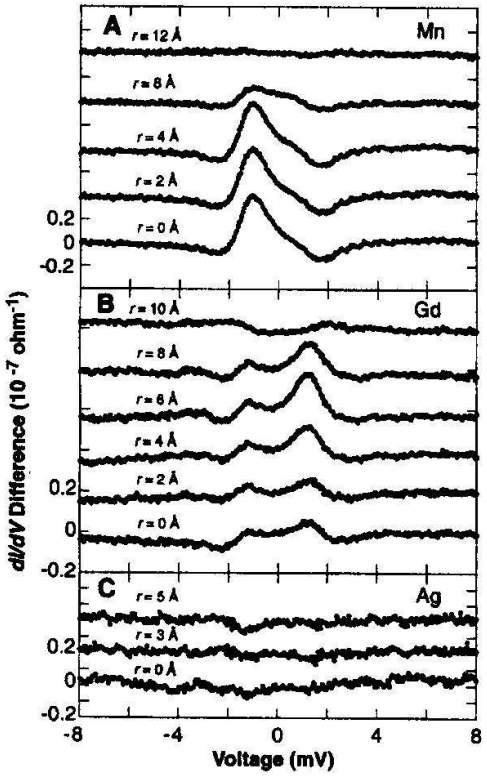

Figure 1.4: Difference spectra measured near an isolated (A) Mn, (B) Gd, and (C) Ag atom [20].

the three kinds of impurity atoms clearly. In these figures, each data for the radial distance from the impurity $r > 0$ is given an offset for clarity. One can clearly see the existence of additional states inside the energy gap near the Mn and Gd atoms, while the difference spectra are zero for all positions around the Ag atom. The tunneling conductance exhibits different particle-hole asymmetry for Mn and Gd atoms.

1.2 BCS Theory

The BCS theory is a microscopic mean-field theory of superconductivity. Assuming translational invariance, this theory is formulated in momentum space, and it can describe homogeneous systems in which momentum $\vec{k}$ is a good quantum number.

The BCS theory is based on the Landau-Fermi liquid theory [21]. In a system with many electrons and ions, effects of strong Coulomb repulsion among conduction electrons are reduced greatly due to their interaction with ions and screening. Since the residual interaction is small, due to the Pauli exclusion principle, only electrons near the Fermi surface are affected by electron-electron interactions substantially. At sufficiently low temperature, the residual interaction can be incorporated by changing the effective mass of those electrons. Thus those electrons can be well described by means of a "free" electron gas model, except that the electrons have an effective mass which is different from that of a "bare" electron. For describing excited states of a normal metal, there is one-to-one correspondence between the states in such a many-electron system and those in a truly free electron gas.

Starting from the Landau-Fermi liquid picture, Cooper studied the problem of a pair of electrons above the Fermi sea interacting via a velocity-dependent non-retarded two-body potential. All but the two electrons are assumed to be noninteracting and to simply block states below the Fermi surface. He found that the lowest-energy state of the two-electron system should be an s-wave state with zero center-of-mass momentum. The total wavefunction must be antisymmetric, so the two electrons must have opposite spin. Thus the concept of a Cooper pair was put forward, where a Cooper pair is formed by two electrons of opposite momenta and spins $\vec{k}\uparrow$ and $-\vec{k}\downarrow$. In conventional superconductors, the size of a Cooper pair can be very large (e.g., about 10,000 Å in Al) in real space so that there is strong overlap of Copper pair wavefunctions. There are strong correlations among them, mainly due to the Pauli exclusive principle. As a result, in the ground state of a superconductor, all Cooper pairs are condensed into a single coherent state. Thus they are not easily scattered by impurities or defects, leading to vanishing resistivity. Furthermore, the "rigidity" of the condensate against magnetic field results in the Meissner state.

The BCS theory is based on the second quantization formulation of quantum mechanics. The creation operator $c^{\dagger}_{\vec{k}\sigma}$ creates an electron in the single-particle state $\vec{k}$ and spin $\sigma =\uparrow$ or $\downarrow$. The destruction operator $c_{\vec{k}\sigma}$ annihilates an electron in the

state $\vec{k}$ and spin $\sigma =\uparrow$ or $\downarrow$. We also define operators $b^\dagger_{\vec{k}}$, $b_{\vec{k}}$ and $n_{\vec{k}\sigma}$ as

$$\begin{aligned} b^\dagger_{\vec{k}} &\equiv c^\dagger_{\vec{k}\uparrow} c^\dagger_{-\vec{k}\downarrow} \,, \\ b_{\vec{k}} &\equiv c_{-\vec{k}\downarrow} c_{\vec{k}\uparrow} \,, \\ n_{\vec{k}\sigma} &\equiv c^\dagger_{\vec{k}\sigma} c_{\vec{k}\sigma} \,. \end{aligned} \tag{1.1}$$

The $b^\dagger_{\vec{k}}$ creates a pair of electrons in the singlet state $\vec{k}\uparrow$ and $-\vec{k}\downarrow$, while the $b_{\vec{k}}$ annihilates such a pair. The $n_{\vec{k}\sigma}$ is the number operator which counts the number of electrons occupying state $\vec{k}\sigma$.

Here we briefly describe the BCS theory for zero temperature. The "reduced" Hamiltonian in the BCS theory is defined by

$$\hat{H}_{red} = \sum_{\vec{k}\sigma} \epsilon_{\vec{k}} n_{\vec{k}\sigma} + \sum_{\vec{k}\vec{k}'} G_{\vec{k}'\vec{k}} b^\dagger_{\vec{k}'} b_{\vec{k}} \,, \tag{1.2}$$

The first term is a sum of kinetic energies of all the electrons and $\epsilon_{\vec{k}}$ is the energy of an electron with momentum $\vec{k}$. The $G_{\vec{k}\vec{k}'}$ is the interaction among Cooper pairs $(\vec{k}\uparrow, -\vec{k}\downarrow)$ and $(\vec{k}'\uparrow, -\vec{k}'\downarrow)$. Although (at $T = 0$), all the electrons are paired up and participate in the superconducting state, only those near the Fermi surface are affected strongly by the electron-phonon interaction. So in this "reduced" model, one considers only those electrons within the Debye energy $\hbar\omega_D$ around the Fermi surface, and take the matrix elements to be zero for all the other electrons. The ground state has no pairing state occupied by a single electron, so the number operator $n_{\vec{k}\sigma} = n_{\vec{k}\uparrow} + n_{-\vec{k}\downarrow}$ can be replaced by

$$n_{\vec{k}\sigma} = 2 b^\dagger_{\vec{k}} b_{\vec{k}} = 2 c^\dagger_{\vec{k}\uparrow} c^\dagger_{-\vec{k}\downarrow} c_{-\vec{k}\downarrow} c_{\vec{k}\uparrow} \,.$$

The Hamiltonian then reduces to

$$\hat{H}_{red} = \sum_{\vec{k}} 2\epsilon_{\vec{k}} b^\dagger_{\vec{k}} b_{\vec{k}} + \sum_{\vec{k},\vec{k}'} G_{\vec{k}'\vec{k}} b^\dagger_{\vec{k}'} b_{\vec{k}} \,. \tag{1.3}$$

It is often argued wrongly that Cooper pairs are bosons and the superconducting state is a Bose condensation, taking $b^\dagger_{\vec{k}}$ ($b_{\vec{k}}$) as the creation (annihilation) operator of a Cooper pair as a boson. This is not the case, however. The strong overlap

and correlations among the Cooper pairs play an important role in forming the superconducting state in a conventional superconductor. The fact that the electrons are fermions and they satisfy the Pauli exclusion principle is the key factor. It can also be seen that $b_{\vec{k}}$ and $b^{\dagger}_{\vec{k}'}$ above do not satisfy the commutation relations for bosons. From their definition (1.1), one finds

$$\begin{aligned} &[b_{\vec{k}}\,, b^{\dagger}_{\vec{k}'}] = 0 && \vec{k} \neq \vec{k}'\,, \\ &[b_{\vec{k}}\,, b^{\dagger}_{\vec{k}'}] = 1 - (n_{\vec{k}\uparrow} + n_{-\vec{k}\downarrow}) && \vec{k} = \vec{k}'\,, \\ &[b_{\vec{k}}\,, b_{\vec{k}'}] = [b^{\dagger}_{\vec{k}}\,, b^{\dagger}_{\vec{k}'}] = 0\,. \end{aligned} \tag{1.4}$$

The term $n_{\vec{k}\uparrow} + n_{-\vec{k}\downarrow}$ above is a result of the Pauli exclusion principle acting on the individual electrons forming a pair. The $b_{\vec{k}}$ and $b^{\dagger}_{\vec{k}}$ describe pairs of fermions.

The BCS theory is a mean-field theory, and for zero temperature, it applies the variational principle. The trial wavefunction for the many-body ground state, $|\psi_0\rangle$, is taken as

$$|\psi_0\rangle = \prod_{\vec{k}} (u_{\vec{k}} + v_{\vec{k}} b^{\dagger}_{\vec{k}})|0\rangle, \tag{1.5}$$

where $|0\rangle$ is a null state. The $u_{\vec{k}}$ is the probability amplitude that the pair state $(\vec{k}, -\vec{k})$ is unoccupied, and $v_{\vec{k}}$ is the probability amplitude that this pair state is occupied. They are variational parameters and satisfy the normalization condition $u^2_{\vec{k}} + v^2_{\vec{k}} = 1$, so that the total wavefunction is normalized. As is clear from Eq. (1.5), the BCS theory is based on ground canonical ensemble, and the number of particles in the system is not conserved. One imposes the constraint that on average the number of electrons is N:

$$\langle\psi_0|\hat{N}_{op}|\psi_0\rangle = \langle\psi_0| \sum_{\vec{k}\sigma} n_{\vec{k}\sigma} |\psi_0\rangle = N\,. \tag{1.6}$$

The $\hat{N}_{op}$ is the number operator which counts the number of electrons in the many-body system. Using the Lagrange multiplier, i.e., chemical potential μ , one minimizes the ground-state energy:

$$\delta W = \delta\langle\psi_0|\hat{H}_{red} - \mu\hat{N}_{op}|\psi_0\rangle = 0\,. \tag{1.7}$$

Substituting the Hamiltonian (1.3) and the wavefunction (1.5) into this equation, and applying the commutation relations of $b^{\dagger}_{\vec{k}}$ and $b_{\vec{k}}$, one has

$$W = \sum_{\vec{k}} 2(\epsilon_{\vec{k}} - \mu) v^2_{\vec{k}} + \sum_{\vec{k}\vec{k}'} G_{\vec{k}\vec{k}'} u_{\vec{k}} v_{\vec{k}} u_{\vec{k}'} v_{\vec{k}'} \,. \tag{1.8}$$

Minimizing this energy in terms of $u_{\vec{k}}$ and $v_{\vec{k}}$, with the normalization condition, one obtains

$$\begin{aligned} u^2_{\vec{k}} &= \frac{1}{2}(1 + \frac{\epsilon_{\vec{k}} - \mu}{E_{\vec{k}}}) \,, \\ v^2_{\vec{k}} &= \frac{1}{2}(1 - \frac{\epsilon_{\vec{k}} - \mu}{E_{\vec{k}}}) \,, \\ u_{\vec{k}} v_{\vec{k}} &= \frac{\Delta_{\vec{k}}}{2E_{\vec{k}}} \,, \end{aligned} \tag{1.9}$$

where $E_{\vec{k}}$ is defined by

$$E_{\vec{k}} \equiv \left[(\epsilon_{\vec{k}} - \mu)^2 + \Delta^2_{\vec{k}} \right]^{1/2} , \tag{1.10}$$

and $\Delta_{\vec{k}}$ satisfy the relation

$$\Delta_{\vec{k}} = -\sum_{\vec{k}'} G_{\vec{k}\vec{k}'} \frac{\Delta_{\vec{k}'}}{2E_{\vec{k}'}} \,. \tag{1.11}$$

The $\Delta_{\vec{k}}$ is called the pairing potential or the order parameter. One must solve $\Delta_{\vec{k}}$ selfconsistently.

When an electron is added to the system in state $\vec{k}\uparrow$, or an electron is removed from state $-\vec{k}\downarrow$, due to the Pauli exclusion principle, the pair state $(\vec{k}\uparrow, -\vec{k}\downarrow)$ is not available for Cooper pairs. This results in an increase ΔW in the total energy of the system,

$$\Delta W = \epsilon_{\vec{k}}(1 - 2v_{\vec{k}})^2 - 2\left(\sum_{\vec{k}'} G_{\vec{k}\vec{k}'} u_{\vec{k}'} v_{\vec{k}'} \right) u_{\vec{k}} v_{\vec{k}} \,. \tag{1.12}$$

Using Eqs. (1.9-1.11), one finds

$$\Delta W = \frac{\epsilon^2_{\vec{k}}}{E_{\vec{k}}} + \frac{\Delta^2_{\vec{k}}}{E_{\vec{k}}} = E_{\vec{k}} \,. \tag{1.13}$$

In the superconducting state, adding an electron in state $\vec{k}\uparrow$ and creating a hole in $-\vec{k}\downarrow$ have identical results, both blocking the pair state $(\vec{k}\uparrow, -\vec{k}\downarrow)$ for Cooper

pairs, except that the total number of electrons differs by two. Thus, in general, a single-particle excitation is a superposition of an electron and a hole: this is called a quasiparticle. The $E_{\vec{k}}$ is the energy of a quasiparticle excitation.

One can define the creation and annihilation operators of quasiparticles, $\gamma^{\dagger}_{\vec{k}\sigma}$ and $\gamma_{\vec{k}\sigma}$, respectively [22, 23] as

$$\begin{aligned}
\gamma^{\dagger}_{\vec{k}\uparrow} &= u_{\vec{k}} c^{\dagger}_{\vec{k}\uparrow} - v_{\vec{k}} c_{-\vec{k}\downarrow} \,, \\
\gamma_{-\vec{k}\downarrow} &= u^{\star}_{\vec{k}} c_{-\vec{k}\downarrow} + v^{\star}_{\vec{k}} c^{\dagger}_{\vec{k}\uparrow} \,, \\
\gamma_{\vec{k}\uparrow} &= u^{\star}_{\vec{k}} c_{\vec{k}\uparrow} - v^{\star}_{\vec{k}} c^{\dagger}_{-\vec{k}\downarrow} \,, \\
\gamma^{\dagger}_{-\vec{k}\downarrow} &= u_{\vec{k}} c^{\dagger}_{-\vec{k}\downarrow} + v_{\vec{k}} c_{\vec{k}\uparrow} \,.
\end{aligned} \tag{1.14}$$

If $|\psi_0\rangle$ has no quasiparticles, one finds

$$\begin{aligned}
\gamma^{\dagger}_{\vec{k}\uparrow}|\psi_0\rangle &= |\psi_{\vec{k}\uparrow}\rangle \,, \\
\gamma^{\dagger}_{-\vec{k}\downarrow}|\psi_0\rangle &= |\psi_{-\vec{k}\downarrow}\rangle \,, \\
\gamma_{\vec{k}\uparrow}|\psi_0\rangle &= 0 \,, \\
\gamma_{-\vec{k}\downarrow}|\psi_0\rangle &= 0 \,.
\end{aligned} \tag{1.15}$$

The quasiparticle operators satisfy the Fermi-Dirac statistics:

$$\{\gamma_{\vec{k}\sigma} \,, \gamma^{\dagger}_{\vec{k}'\sigma'}\} = \delta_{\vec{k}\vec{k}'}\delta_{\sigma\sigma'} \,, \tag{1.16}$$

$$\{\gamma_{\vec{k}\sigma} \,, \gamma_{\vec{k}'\sigma'}\} = \{\gamma^{\dagger}_{\vec{k}\sigma} \,, \gamma^{\dagger}_{\vec{k}'\sigma'}\} = 0 \,. \tag{1.17}$$

In general, the order parameter is a function of momentum, reflecting the nature of the pairing interaction. In an isotropic s-wave superconductor, one can assume that the interaction strength is independent of momentum, $G_{\vec{k}\vec{k}'} \equiv G$. Then $\Delta_{\vec{k}}$ in Eq. (1.13) is a constant, $\Delta_{\vec{k}} \equiv \Delta(T)$, and $\Delta(T)$ is called the energy gap at temperature T. As can be seen in Eq. (1.13), it is the minimum energy required to create a quasiparticle. For such an isotropic case, the excitation energy $E_{\vec{k}}$ is illustrated as a function of momentum magnitude k in Fig. 1.5 [24], in which $\Delta_0 \equiv \Delta(T)$.

In the superconducting ground state, there is no single-particle state within the energy gap, as illustrated in Fig. 1.6 [25]. As the number of states must be conserved,

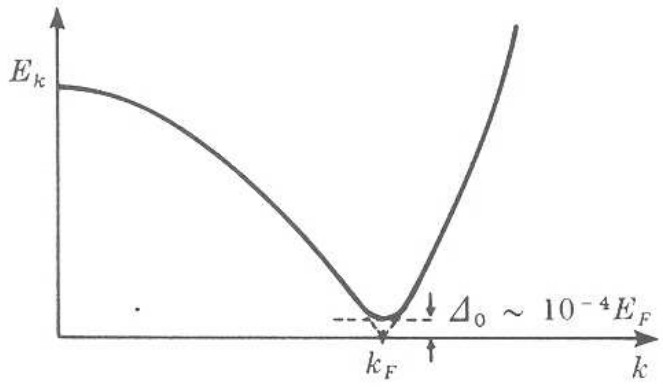

Figure 1.5: Quasiparticle excitation energy as a function of momentum k. The k_F and E_F are the Fermi momentum and Fermi energy, respectively [24].

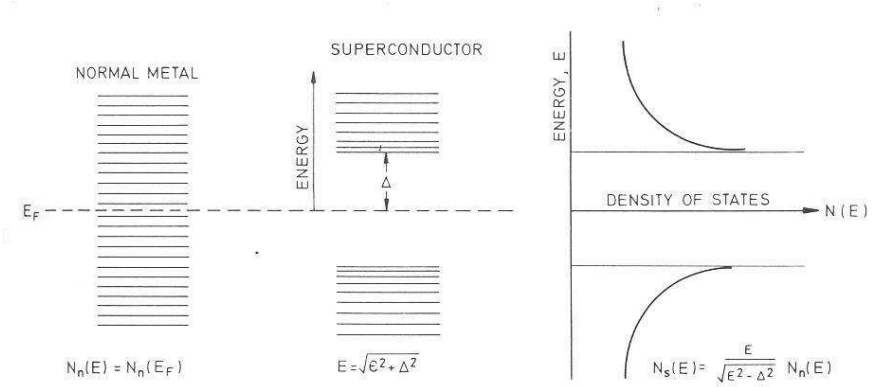

Figure 1.6: In the superconducting state, energy gap is created around $E = E_F$. The ϵ is the single-particle kinetic energy measured from E_F. The $N_n(E)$ and $N_s(E)$ are the DOS in the normal state and superconducting state, respectively [25].

the states inside the gap in the normal state are pushed outside the gap in the superconducting state. Thus the single-particle density of state (DOS) has a peak at the gap edge, called the coherence peak, as shown in Fig. 1.6. Experimentally, one can measure the energy gap and excitation spectrum, for example, by tunneling electrons or holes into the superconductor. STM can tunnel electrons or holes at different positions and in different directions. In a homogeneous isotropic system, the DOS should be independent of position and momentum.

For finite temperature, the BCS theory is formulated on the basis of the statistical method for a ground canonical ensemble. One of the predictions deducted from the

BCS theory that agrees perfectly with experiments, is the temperature dependence of the energy gap. This is illustrated in Fig. 1.7. The temperature-dependent gap $\Delta(T)$ measured in units of the zero temperature gap $\Delta_0 = \Delta(0)$ is almost unity for $T \lesssim 0.4\, T_c$. As T increases further, it decreases rapidly and continuously to zero at $T = T_c$, signaling a second-order phase transition. This behavior is universal for many different conventional, weak-coupling superconductors (circles in Fig. 1.7), and agrees very well with the theory.

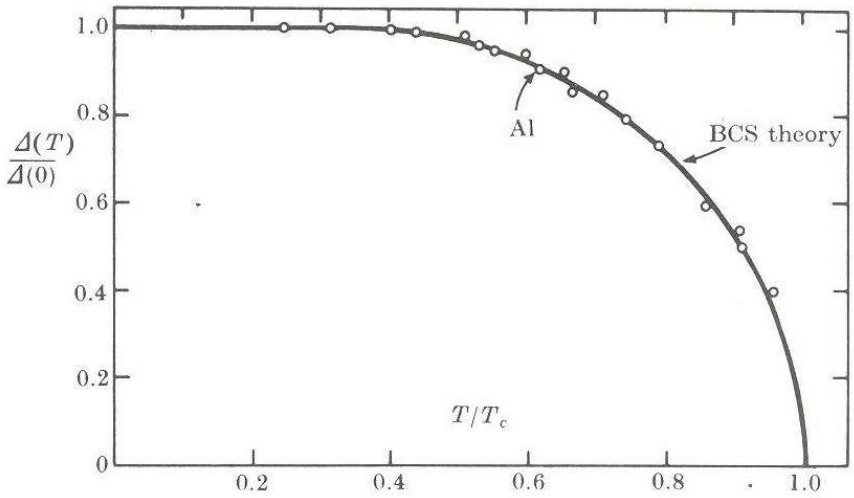

Figure 1.7: Temperature dependance of measured energy gap for various conventional superconductors. The curve is the BCS prediction [9].

1.3 BdG Theory

The Bogoliubov-de Gennes (BdG) theory [9] is a generalization of the BCS theory, formulated in real space. The starting point of this theory is to define the creation and annihilation operators Ψ and $\Psi^\dagger$ respectively, in real space:

$$\begin{aligned} \Psi(\vec{r}\sigma) &= \sum_{\vec{k}} e^{i\vec{k}\cdot\vec{r}} c_{\vec{k}\sigma}\,, \\ \Psi^\dagger(\vec{r}\sigma) &= \sum_{\vec{k}} e^{-i\vec{k}\cdot\vec{r}} c^\dagger_{\vec{k}\sigma}\,. \end{aligned} \tag{1.18}$$

Here $c^\dagger_{\vec{k}\sigma}$ and $c_{\vec{k}\sigma}$ are the creation and annihilation operators defined in momentum space in the BCS theory. The $\Psi(\vec{r}\sigma)^\dagger$ ($\Psi(\vec{r}\sigma)$) creates (removes) an electron with

spin $\sigma =\uparrow$ or $\downarrow$ from position $\vec{r}$. Assuming a point interaction in real space to describe s-wave coupling with coupling constant g, the Hamiltonian $\hat{H}$ can be written as

$$\begin{aligned}
\hat{H} &= \hat{H}_0 + \hat{H}_1 \,, \\
\hat{H}_0 &= \int d\vec{r} \sum_{\sigma} \Psi^{\dagger}(\vec{r}\sigma) \left[\frac{\hat{p}^2}{2m_e} + U_0(\vec{r}) \right] \Psi(\vec{r}\sigma) \,, \\
\hat{H}_1 &= -\frac{1}{2} g \int d\vec{r} \sum_{\sigma\sigma'} \Psi^{\dagger}(\vec{r}\sigma)\Psi^{\dagger}(\vec{r}\sigma')\Psi(\vec{r}\sigma')\Psi(\vec{r}\sigma) \,,
\end{aligned} \tag{1.19}$$

where $\hat{p}$ is the momentum operator. The $\hat{H}_0$ above is a sum of the kinetic energy and single-particle potential energy with the mass of an electron m_e. The $U_0(\vec{r})$ incorporates crystal potentials and external potentials as due to impurities. The $\hat{H}_1$ models the electron-phonon interaction among Cooper pairs.

In mean-field approximation, one rewrites the interaction in terms of effective two-body interactions:

$$\begin{aligned}
\hat{H}_{eff} = \int d\vec{r} \Bigg[\sum_{\sigma} \Psi^{\dagger}(\vec{r}\sigma)\hat{H}_e(\vec{r})\Psi(\vec{r}\sigma) + U(\vec{r})\Psi^{\dagger}(\vec{r}\sigma)\Psi(\vec{r}\sigma) \\
+ \Delta(\vec{r})\Psi^{\dagger}(\vec{r}\uparrow)\Psi^{\dagger}(\vec{r}\downarrow) + \Delta^{\star}(\vec{r})\Psi(\vec{r}\downarrow)\Psi(\vec{r}\uparrow) \Bigg] \,,
\end{aligned} \tag{1.20}$$

where

$$\hat{H}_e = \frac{\hat{p}^2}{2m_e} + U_0(\vec{r}) - \mu \,. \tag{1.21}$$

Here we have introduced the chemical potential μ as in the BCS theory. The $U(\vec{r})$ is the Hartree-Fock potential arising from the pairing interaction. The last two terms in Eq. (1.20) are called anomalous terms, representing Cooper pair scattering. It may be noted that, both of the two terms change the number of particles by two. The $\Delta(\vec{r})$ is the order parameter or the pairing potential, now depending on position $\vec{r}$.

We diagonalize the effective Hamiltonian

$$\hat{H}_{eff} = E_g + \sum_{n,\sigma} E_n \gamma^{\dagger}_{n\sigma}\gamma_{n\sigma} \,, \tag{1.22}$$

where E_g is the ground state energy. The $\gamma^{\dagger}_{n\sigma}$ and $\gamma_{n\sigma}$ are the creation and annihilation operators of quasiparticle with quantum number n and spin σ, and E_n is the

energy eigenvalue of the quasiparticle excitation. The diagonalization is made via a unitary transformation,

$$\begin{aligned}\Psi^{\dagger}(\vec{r}\uparrow) &= \sum_{n}\left(u_{n}^{\star}\gamma_{n\uparrow}^{\dagger} - v_{n}\gamma_{n\downarrow}\right), \\ \Psi(\vec{r}\downarrow) &= \sum_{n}\left(v_{n}^{\star}\gamma_{n\uparrow}^{\dagger} + u_{n}\gamma_{n\downarrow}\right).\end{aligned} \tag{1.23}$$

It is to be noted that, in analogy to Eq. (1.14), the u_n and v_n are the amplitudes of the electron and hole parts of a quasiparticle with quantum number n, respectively. Here $\gamma_{n\sigma}$ and $\gamma_{n\sigma}^{\dagger}$ still satisfy the fermion anti-commutation relations, similarly to Eq. (1.17). Using Eq. (1.22) and the anti-commutation relation of $\gamma_{n\sigma}$ and $\gamma_{n\sigma}^{\dagger}$, one has

$$\begin{aligned}[\hat{H}_{eff}, \gamma_{n\sigma}] &= -E_{n}\gamma_{n\sigma}\,, \\ [\hat{H}_{eff}, \gamma_{n\sigma}^{\dagger}] &= E_{n}\gamma_{n\sigma}^{\dagger}\,,\end{aligned} \tag{1.24}$$

and

$$\begin{aligned}[\Psi(\vec{r}\uparrow), \hat{H}_{eff}] &= [\hat{H}_{e} + U(r)]\Psi(\vec{r}\uparrow) + \Delta(r)\Psi^{\dagger}(\vec{r}\downarrow)\,, \\ [\Psi(\vec{r}\downarrow), \hat{H}_{eff}] &= [\hat{H}_{e} + U(r)]\Psi(\vec{r}\downarrow) - \Delta^{\star}(r)\Psi^{\dagger}(\vec{r}\uparrow)\,.\end{aligned} \tag{1.25}$$

From Eqs. (1.23-1.25),

$$\begin{aligned}\left[\hat{H}_{e} + U(\vec{r})\right]u_{n}(\vec{r}) + \Delta(\vec{r})v_{n}(\vec{r}) &= E_{n}u_{n}(\vec{r})\,, \\ -\left[\hat{H}_{e}^{\star} + U(\vec{r})\right]v_{n}(\vec{r}) + \Delta^{\star}(\vec{r})u_{n}(\vec{r}) &= E_{n}v_{n}(\vec{r})\,.\end{aligned} \tag{1.26}$$

These are Schrödinger-like equations for the electron and hole amplitudes, u and v, of a quasiparticle, which are called the BdG equations. The $\Delta(\vec{r})$ can be considered as a pairing potential that couples the electron and hole components. It is important to realize the difference between $\Delta(\vec{k})$ in the BCS theory and $\Delta(\vec{r})$ in the BdG theory. The former is the energy gap to create a quasiparticle excitation in state $\vec{k}$, while the latter cannot be considered as the "energy gap", since it is a function of position. Nevertheless, $\Delta(\vec{r})$ signifies the ordering of the superconductor at position $\vec{r}$.

By minimizing the free energy, one obtains

$$U(\vec{r}) = -g\sum_{n}\left[|u_{n}(\vec{r})|^{2}f(E_{n}) + |v_{n}(\vec{r})|^{2}(1 - f(E_{n}))\right], \tag{1.27}$$

$$\Delta(\vec{r}) = +g\sum_{0\leq\epsilon_{n}\leq\hbar\omega_{D}} v_{n}^{\star}(\vec{r})u_{n}(\vec{r})(1 - 2f(E_{n})), \tag{1.28}$$

where f is the Fermi-Dirac distribution function,

$$f(E_n) = \left(e^{(E_n-\mu)/k_BT} + 1\right)^{-1}, \tag{1.29}$$

with k_B the Boltzmann constant. As in the BCS theory, we assume that the electron-phonon interaction is nonzero only for the electrons around the Fermi surface within energy $\mu \pm \hbar\omega_D$. Equation (1.28) is called the gap equation. Throughout this work, we consider isotropic s-wave pairing. In this case, there is no Fock (exchange) interaction and the Hartree interaction simply shifts the energy levels. Therefore the Hartree-Fock potential U is neglected in this thesis.

The Eqs. (1.26) and (1.28) must be solved selfconsistently. One starts out solving Eq. (1.26) by assuming some form of $\Delta(\vec{r})$, then construct the new potential from Eq. (1.28), and then solve Eq. (1.26) with new $\Delta(\vec{r})$, and so on. The process is iterated until selfconsistency is attained. Once selfconsistency is achieved, one can calculate the LDOS and the tunneling conductance,

$$A(E, \vec{r}) = \sum_n \Big[|u_n(\vec{r})|^2 \delta(E - E_n) + |v_n(\vec{r})|^2 \delta(E + E_n) \Big], \tag{1.30}$$

$$\frac{\partial I(eV, \vec{r})}{\partial V} \propto -\sum_n \Big[|u_n(\vec{r})|^2 f'(E_n - eV) + |v_n(\vec{r})|^2 f'(E_n + eV) \Big], \tag{1.31}$$

where E and V are the energy and applied bias voltage, respectively. The δ is the Kronecker delta function. The f' is the first derivative of the Fermi-Dirac function.

The BdG equations solve for all the single-particle states. Typically, $\hbar\omega_D$ is a few times the energy gap, and for a weak-coupling superconductor, $\hbar\omega_D$ and the energy gap are of the order of milli-electron-volt, meV. The μ, on the other hand, can be as large as tens of electron volt (e.g. 12 eV for Al). For such a large μ, solving the BdG equations exactly and selfconsistently can be a formidable task. In the work for this thesis, we have solved the BdG equations directly and numerically, by utilizing parallel computation. The procedure of our parallel computation is discussed in Appendix A.

Chapter 2

Electronic Structure around a Vortex

2.1 Motivation

In this chapter, electronic structure around an isolated vortex in the superconductor $NbSe_2$ is explored within the framework of the BdG theory. The purpose of this work is to construct programs for solving the BdG equations selfconsistently for the well-known problem of a single vortex, and to check that our codes work correctly by comparison with the results of GS [26] and the experiment [12]. Furthermore, the local effects of a vortex on superconductivity are expected to be similar to those of a magnetic impurity in that they both tend to suppress superconductivity locally. So the work presented in this chapter is a preliminary study to help us better understand the effects of local magnetic field.

In Sec.2.2, parameter values of $NbSe_2$, for which we investigate the vortex problem, are explained. In Sec.2.3, our BdG programs are checked for the simplest case, i.e., for a homogeneous system for which the well-known BCS results are available. In Sec.2.3, electronic structure around a vortex is studied.

2.2 Material

The calculations are performed for the conventional weak-coupling type-II superconductor, $NbSe_2$. High-quality single crystals of $NbSe_2$ are readily available, and easy to cleave for a clean surface ideal for STM. It is the first material from which direct images of vortex states were obtained [11]. $NbSe_2$ is a layered compound and its Fermi surface can be well approximated to be a cylinder along the k_z direction in

momentum space. Thus for the vortex problem, we assume cylindrical symmetry and solve the problem for a two-dimensional system. Another advantage for BdG calculation is that its Fermi energy, E_F, is relatively small. (Difficulty arising from large E_F is discussed in Section 3.2.2.) The effects of crystal potential U_0 can be incorporated in terms of the effective mass $m_\rho \equiv 2m_e$. $\Delta_0 = 1.2$ meV, $T_C = 8.2$ K, and E_F =38.5 meV.

2.3 Homogeneous System

2.3.1 Formulation

In a homogeneous system, the order parameter $\Delta(\vec{r})$ is a constant $\Delta(\vec{r}) \equiv \Delta$. Thus the BdG equations can be written as

$$\begin{pmatrix} \hat{H}_e & \Delta \\ \Delta & -\hat{H}_e^\star \end{pmatrix} \begin{pmatrix} u_n(\vec{r}) \\ v_n(\vec{r}) \end{pmatrix} = E_n \begin{pmatrix} u_n(\vec{r}) \\ v_n(\vec{r}) \end{pmatrix} , \tag{2.1}$$

where

$$\hat{H}_e = \frac{\hat{p}^2}{2m_\rho} - E_F. \tag{2.2}$$

For all the results shown in this thesis, we neglect change in the chemical potential from E_F at finite temperature. Assuming cylindrical symmetry, the problem can be solved in terms of circular cylindrical coordinates (r,θ), and one can separate the nodal and angular wavefunctions :

$$\begin{aligned} u_n(\vec{r}) &= u_{\nu,l}(r)e^{il\theta} , \\ v_n(\vec{r}) &= v_{\nu,l}(r)e^{il\theta} , \end{aligned} \tag{2.3}$$

where $\nu = 0, 1, 2, \cdots$ is the nodal quantum number and $l = 0, \pm1, \pm2, \cdots$ is the angular momentum quantum number. Using Eqs. (2.3), the BdG equations can be simplified to equations for the radial part of the quasiparticle wavefunctions:

$$\begin{pmatrix} \hat{H}_r & \Delta \\ \Delta & -\hat{H}_r^\star \end{pmatrix} \begin{pmatrix} u_{\nu,l}(r) \\ v_{\nu,l}(r) \end{pmatrix} = E_{\nu,l} \begin{pmatrix} u_{\nu,l}(r) \\ v_{\nu,l}(r) \end{pmatrix} , \tag{2.4}$$

where $\hat{H}_r = -\frac{\hbar^2}{2m_\rho}\left[\frac{1}{r}\frac{d}{dr}\left(r\frac{d}{dr}\right) - \frac{l^2}{r^2}\right] - E_F$. We choose the phase of the wavefunctions so that $u(r)$ and $v(r)$ are real.

In the normal state, $\Delta \equiv 0$, and the BdG equations reduce to two Schrödinger equations for a hole and a particle. For a finite system of radius R, the wavefunctions are,

$$\phi_{m,l}(r) = \frac{\sqrt{2}}{R} J_l(\alpha_{m,l}\frac{r}{R})/J_{l+1}(\alpha_{m,l}), \tag{2.5}$$

which are normalized in a disc of radius R. Here $\alpha_{m,l}$ is the m-th zero of the Bessel function of order l, J_l ($m = 1, 2, \cdots$). In the superconducting state, we expand the quasiparticle amplitudes in terms of the complete orthonormal set of the wavefunctions in the normal state:

$$\begin{aligned} u_{\nu,l}(r) &= \sum_m c_{\nu,m}\phi_{m,l}(r), \\ v_{\nu,l}(r) &= \sum_m d_{\nu,m}\phi_{m,l}(r). \end{aligned} \tag{2.6}$$

In a weak-coupling superconductor, only those states close to the Fermi surface are relevant to superconductivity and the states with energy within $\pm\hbar\omega_D$ (around E_F) are needed in the gap equation. Thus in this expansion, only the states with energies below $E_F + \epsilon$ are included, where ϵ is of the order of $\hbar\omega_D$. Therefore the node number m varies from 1 to N_l, where N_l is the maximum node number for a given angular momentum l, defined by

$$\frac{\hbar^2\alpha_{N_l,l}^2}{2m_\rho R^2} \leq E_F + \epsilon\,. \tag{2.7}$$

In our calculation, ϵ is taken to be $2\hbar\omega_D$. Higher cutoff energy gives the same results. Substituting Eq. (2.6) into Eqs. (2.1), the BdG equations are reduced to a $2N_l \times 2N_l$ matrix equation for the expansion coefficients for each angular momentum l:

$$\begin{pmatrix} T & \widetilde{\Delta} \\ \widetilde{\Delta} & -T \end{pmatrix} \psi_{\nu,l} = E_{\nu,l}\psi_{\nu,l}\ , \tag{2.8}$$

where $\psi_{\nu,l}^T = (c_{\nu,1}, \cdots, c_{\nu,N_l}, d_{\nu,1}, \cdots, d_{\nu,N_l})$, and $\widetilde{\Delta} = \Delta\mathbf{I}$ with $\mathbf{I}$ the identity matrix.

Due to orthonormality of the Bessel functions, the matrix elements are given by

$$\begin{aligned} T_{m,m'} &= \langle m, l|\hat{H}_r|m', l\rangle \\ &= \left(\frac{\hbar^2\alpha_{m,l}^2}{2m_\rho} - E_F\right)\delta_{m,m'}\,, \end{aligned} \tag{2.9}$$

and

$$\begin{aligned}\widetilde{\Delta}_{m,m'} &= \langle m, l|\Delta|m', l\rangle \\ &= \Delta\delta_{m,m'}\,.\end{aligned} \tag{2.10}$$

One solves the eigenvalue problem Eq. (2.8) for all l to obtain states below energy $E_F + \epsilon$. The order parameter is reconstructed through the gap equation (1.29),

$$\Delta(r) = g \sum_{0\le E_{\nu,l}\le\hbar\omega_D} u_{\nu,l}(r)v_{\nu,l}(r)[1 - 2f(E_{\nu,l})], \tag{2.11}$$

where g is the coupling constant. During an iteration, for each angular momentum l, solving the matrix (2.8) and calculating the contribution to Δ are a process independent of other values of l, and calculation for different values of l can be performed in parallel. The flow chart of parallel computation is described in Sec. A.2 in Appendix A. The numerical method for solving the matrix equation is discussed in Sec. A.3.1 .

2.3.2 Results and Discussion

Results for a homogeneous system of clean $NbSe_2$ are presented for $R = 10,000$ a.u.. For programming, we use the boundary radius R (in units of a.u. which is 0.5292 Å) and the bulk zero-temperature energy gap $\Delta_0 = 1.2$ meV as the length and energy unit, respectively. The coupling constant g is about 3 meV·Å for $R = 10,000$ a.u. and $\hbar\omega_D$ is taken to be 3 meV, which yields $T_c \approx 8.2$ K.

Figure 2.1 shows the tunneling conductance dI/dV of a pure $NbSe_2$ sample as a function of voltage V for temperature T = 1 K, 2 K, 5 K, and 7 K. We have confirmed that both dI/dV and LDOS are independent of position r, as expected for a homogeneous system. We have performed calculation for T =0.1 K and have found that the result is almost the same as for T =1 K. In Fig. 2.1, the existence of the energy gap $\Delta \equiv \Delta(T)$ around the Fermi surface $eV/\Delta_0 = 0$ and the coherence peak at $eV/\Delta_0 \pm 1$, can be seen clearly. As temperature is increased, more and more quasiparticles are created (for a given voltage), which results in a smaller energy gap. Accordingly, more states are created inside Δ_0 and thus the coherence peak height is reduced. As T reaches $T_c = 8.2$ K, superconductivity is destroyed totally, the energy

gap ceases to exist and the density of states (LDOS and dI/dV) becomes flat as a function of energy. Note that in a free electron gas in two dimensions (in the normal state), the bulk DOS is a constant.

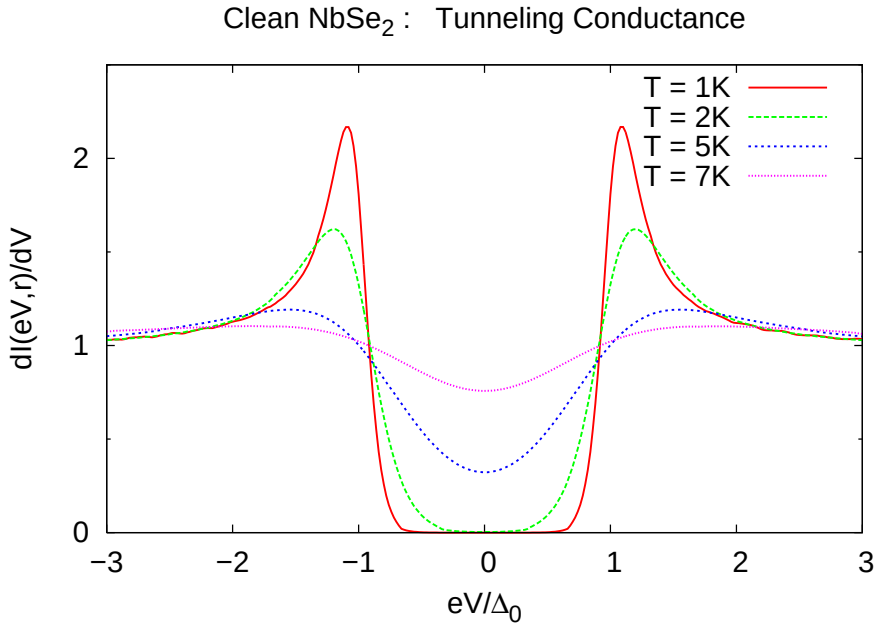

Figure 2.1: Normalized tunneling conductance of a pure $NbSe_2$ at temperature T = 1 K, 2 K, 5 K and 7 K.

The LDOS for the homogeneous system is shown in Fig. 2.2. Here for presentation purpose each delta function in Eq. (1.30) has been replaced by a normalized Gaussian of width γ,

$$\delta(eV \pm E_n) = \frac{1}{\gamma\sqrt{\pi}} \exp\left[-\left(\frac{eV \pm E_{\rm n}}{\gamma}\right)^2\right], \tag{2.12}$$

with $\gamma = 0.1$. For $T = 1$ K and 2 K, the LDOS is identical. Apparently, the energy gap decreases rather slowly as temperature is reduced, for $T \lesssim 5$ K. To see the temperature dependance more clearly, we show in Fig. 2.3 the uniform order parameter $\Delta(T)$ as a function of temperature T. The smooth, slow decrease of the gap as T increases can be seen: Δ reaches a half of Δ_0 at $T \approx 7.5$ K and the gap closes rapidly as T approaches to T_c. This behavior is consistent with the BCS theory shown in Fig. 1.7. The BCS theory gives an analytical formula for Δ as a function of T for $T \approx T_C$ [27] as

$$\Delta(T) \approx 1.74\Delta_0\sqrt{1 - \frac{T}{T_C}}\,. \tag{2.13}$$

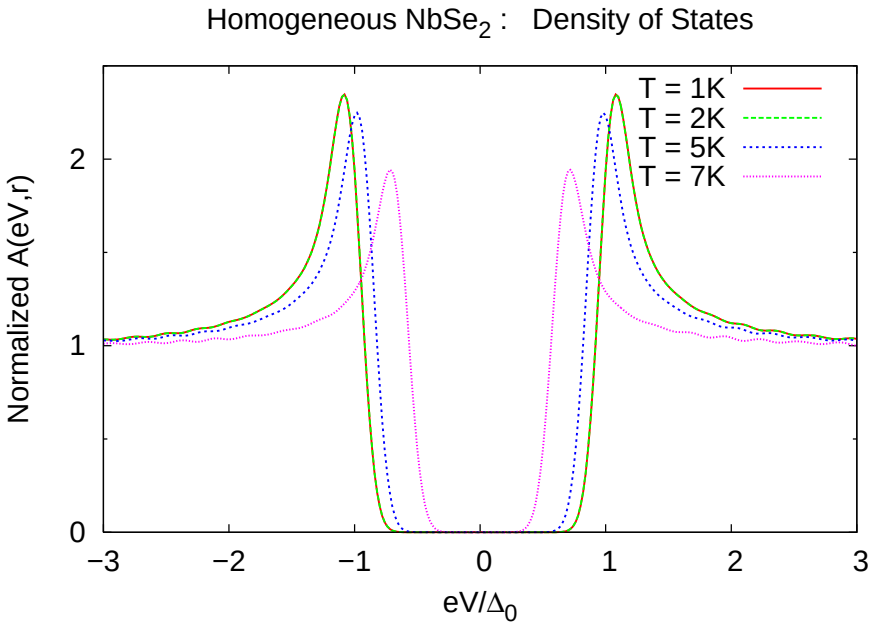

Figure 2.2: LDOS of a pure $NbSe_2$ at temperature T = 1 K, 2 K, 5 K and 7 K.

Our result yields this behavior as indicated in Fig. 2.3, where the BCS formula above is plotted in the dashed curve.

2.4 Isolated Vortex

2.4.1 Formulation

The BdG equations in the presence of magnetic field are

$$\begin{pmatrix} \hat{H}_e & \Delta(\vec{r}) \\ \Delta^\star(\vec{r}) & -\hat{H}_e^\star \end{pmatrix} \begin{pmatrix} u_n(\vec{r}) \\ v_n(\vec{r}) \end{pmatrix} = E_n \begin{pmatrix} u_n(\vec{r}) \\ v_n(\vec{r}) \end{pmatrix}, \tag{2.14}$$

with the single-particle Hamiltonian

$$\hat{H}_e = \frac{1}{2m_\rho}\left(\hat{p} - \frac{e}{c}\vec{A}(\vec{r})\right)^2 - E_F,$$

where $\vec{A}(\vec{r})$ is the vector potential. The $\hat{H}_e$ depends on the choice of $\vec{A}$, which is not unique. However, under a gauge transformation,

$$\vec{A}' = \vec{A} + \nabla\chi(\vec{r}), \tag{2.15}$$

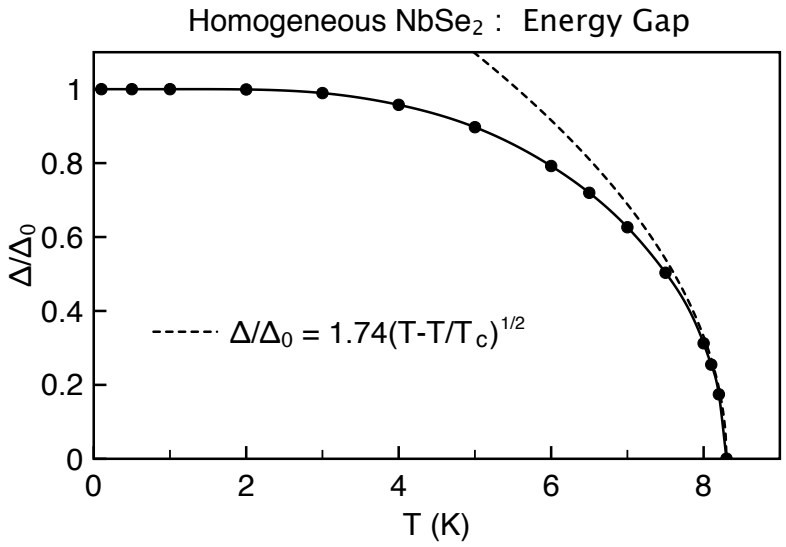

Figure 2.3: Uniform order parameter Δ as a function of temperature.

all physical observables must be invariant. The quasiparticle wavefunctions are transformed by such a gauge transformation to

$$\begin{pmatrix} u_n'(\vec{r}) \\ v_n'(\vec{r}) \end{pmatrix} = \begin{pmatrix} u_n(\vec{r})\exp[\frac{ie}{\hbar c}\chi] \\ v_n(\vec{r})\exp[-\frac{ie}{\hbar c}\chi] \end{pmatrix}, \tag{2.16}$$

and the order parameter changes to

$$\Delta'(\vec{r}) = \Delta(\vec{r})e^{\frac{2ie}{\hbar c}\chi(\vec{r})}\,. \tag{2.17}$$

One can show that u_n', v_n', and Δ' satisfy the BdG equations of the same form as Eq. (2.14), and thus the quasiparticle eigenvalues are gauge invariant. The self-consistent pairing potential $\Delta(\vec{r})$ must be a single-valued function of $\vec{r}$, no matter what gauge one takes. For example, in a cylindrically symmetric system, the gauge function must be of the form

$$\chi = \frac{\hbar c}{2e} m\theta, \tag{2.18}$$

where θ is the azimuthal angle in two-dimensional polar coordinates, and m is an integer.

Consider an isolated vortex passing through $r = 0$ along the z direction. To model $NbSe_2$, we assume cylindrical symmetry and isotropic s-wave pairing. It is

convenient to choose a gauge so that

$$\Delta(\vec{r}) = |\Delta(r)|e^{-i\theta}. \tag{2.19}$$

One can eliminate the phase with a gauge transformation with

$$\chi = \frac{\hbar c}{2e}\theta. \tag{2.20}$$

Thus the new pairing potential is

$$\Delta'(\vec{r}) = |\Delta(r)|. \tag{2.21}$$

The flux quantization, namely the fact that a vortex encloses a quantum of magnetic flux, $\phi_0 = \frac{hc}{2e}$, is a direct consequence of the single-valuedness of the pairing potential, which corresponds to the Cooper-pair wavefunction in the GL theory. The flux quantization has been confirmed experimentally [28, 29, 30]. In general, a vortex can carry multiple flux quanta. In the vortex lattice in a bulk system, however, the most energetically favorable state is such that each vortex carries only one flux quantum [15]. Recently, vortices carrying multiple flux quanta have been observed in mesoscopic superconductors, in which the system size is comparable to the coherence length [31, 32, 33, 34, 15].

$NbSe_2$ is strongly type-II with $\kappa \approx 10$ ($\lambda \approx 1400$ Å, $\xi \approx 140$ Å) [35, 36, 37], and one can assume that the magnetic field around a vortex is constant. Thus in our BdG equations, we ignore the vector potential, and the equations are

$$\begin{pmatrix} \hat{H}_e & \Delta(r) \\ \Delta^\star(r) & -\hat{H}_e^\star \end{pmatrix} \begin{pmatrix} u_n(\vec{r}) \\ v_n(\vec{r}) \end{pmatrix} = E_n \begin{pmatrix} u_n(\vec{r}) \\ v_n(\vec{r}) \end{pmatrix}, \tag{2.22}$$

where $\hat{H}_e = -\frac{\hbar^2}{2m_\rho}\left[\frac{1}{r}\frac{\partial}{\partial r}\left(r\frac{\partial}{\partial r}\right) + \frac{1}{r^2}\frac{\partial^2}{\partial\theta^2}\right] - E_F$. The angular momentum l is a good quantum number under cylindrical symmetry, so one can separate the wavefunctions into the radial and angular parts,

$$\begin{pmatrix} u_n(\vec{r}) \\ v_n(\vec{r}) \end{pmatrix} = \begin{pmatrix} u_{\nu,l}(r)e^{i(l-\frac{1}{2})\theta} \\ v_{\nu,l}(r)e^{i(l+\frac{1}{2})\theta} \end{pmatrix}, \tag{2.23}$$

where $l = \pm\frac{1}{2}, \pm\frac{3}{2}, \pm\frac{5}{2}, \cdots$. Using Eqs. (2.23), the BdG equations can be simplified to equations for the radial part of the quasiparticle wavefunctions:

$$\begin{pmatrix} \hat{H}_r^- & |\Delta(r)| \\ |\Delta(r)| & -\hat{H}_r^+ \end{pmatrix} \begin{pmatrix} u_{\nu,l}(r) \\ v_{\nu,l}(r) \end{pmatrix} = E_{\nu,l} \begin{pmatrix} u_{\nu,l}(r) \\ v_{\nu,l}(r) \end{pmatrix}, \tag{2.24}$$

where $\hat{H}_r^{\pm} = -\frac{\hbar^2}{2m_\rho}\left[\frac{1}{r}\frac{d}{dr}\left(r\frac{d}{dr}\right) - \frac{(l\pm 1/2)^2}{r^2}\right] - E_F$. The following steps to deal with the BdG equations are similar to those used in the homogeneous problem. We expand the radial part of the quasiparticle amplitudes, $u_n(r)$ and $v_n(r)$, in terms of the complete orthonormal set of the Bessel functions which are normalized in a disc of radius R:

$$\begin{aligned} u_{\nu,l}(r) &= \sum_k c_{\nu,k}\phi_{k,l-1/2}(r), \\ v_{\nu,l}(r) &= \sum_k d_{\nu,k}\phi_{k,l+1/2}(r), \end{aligned} \tag{2.25}$$

where $\phi_{k,l'}(r) = \frac{\sqrt{2}}{R}J_{l'}(\alpha_{k,l'}\frac{r}{R})/J_{l'+1}(\alpha_{k,l'})$ with $l' = l \pm \frac{1}{2}$ an integer. Only the states below the cutoff energy $E_F + 2\hbar\omega_D$ are included in our calculation (higher cutoff energy gives the same results), and the cutoff energy determines the maximum l and N_l. By substituting Eq. (2.25) into Eq. (2.24), we have a matrix equation of dimension $2N_l \times 2N_l$ for each angular momentum l:

$$\begin{pmatrix} T^- & \widetilde{\Delta} \\ \widetilde{\Delta}^T & -T^+ \end{pmatrix} \psi_{\nu,l} = E_{\nu,l}\psi_{\nu,l}, \tag{2.26}$$

where $\psi_{\nu,l}^T = (c_{\nu,1}, ..., c_{\nu,N_l}, d_{\nu,1}, ..., d_{\nu,N_l})$. Due to orthonormality of the Bessel functions, the matrix elements are reduced to

$$\begin{aligned} T^-_{k,k'} &= \langle k, l-\frac{1}{2}|\hat{H}_r^-|k', l-\frac{1}{2}\rangle \\ &= \left(\frac{\hbar^2\alpha^2_{k,l-\frac{1}{2}}}{2m_\rho} - E_F\right)\delta_{k,k'} \quad , \\ T^+_{k,k'} &= \langle k, l+\frac{1}{2}|\hat{H}_r^+|k', l+\frac{1}{2}\rangle \\ &= \left(E_F - \frac{\hbar^2\alpha^2_{k,l+\frac{1}{2}}}{2m_\rho}\right)\delta_{k,k'} \quad , \end{aligned} \tag{2.27}$$

and

$$\begin{aligned}\widetilde{\Delta}_{k,k'} &= \langle k, l-\frac{1}{2}|\Delta(r)|k', l+\frac{1}{2}\rangle \\ &= \int_0^\infty r\,dr\,\phi_{k,l-\frac{1}{2}}(r)|\Delta(r)|\phi_{k',l+\frac{1}{2}}(r).\end{aligned} \tag{2.28}$$

The BdG equations are invariant under the transformation,

$$\begin{aligned}u_{\nu,l}(\vec{r}) &\longrightarrow v^\star_{\nu,-l}(\vec{r}), \\ v_{\nu,l}(\vec{r}) &\longrightarrow -u^\star_{\nu,-l}(\vec{r}), \\ E_{\nu,l} &\longrightarrow -E_{\nu,-l}.\end{aligned} \tag{2.29}$$

In our system, this means that a *positive*-energy state for *negative* angular momentum $-l$ and energy $E_{\nu,-l}$ is equivalent to the *negative*-energy state for *positive* l and energy $E_{\nu,l} = -E_{\nu,-l}$. Therefore, one can cut the computational time almost by half by obtaining positive- and negative-energy solutions for positive l only.

As in the homogeneous case, we perform calculation according to the flow chart in Fig A.4 in Sec. A.2 in Appendix A, until selfconsistency is achieved. The numerical procedure for evaluation of the matrix elements is discussed in Sec. A.3.2 . The order parameter is calculated at a discrete set of positions, while calculation of the matrix elements in Eq. (2.28) requires $\Delta(r)$ as a smooth function of r. So curve fitting, which is described in Appendix B, is applied.

2.4.2 Results and Discussion

We present results for the same parameter values as for the homogeneous case. Figure 2.4 shows the converged order parameter $\Delta(r)$ as a function of radial coordinate r for various temperatures. It can be seen that the order parameter is suppressed to zero at the center of the vortex and gradually recovers to the bulk value as r increases. In the macroscopic picture of the GL theory, $\Delta(\vec{r})$ corresponds to the Cooper pair wavefunction. The spatial distribution of the order parameter indicates that Cooper pairs are broken up and superconductivity is suppressed around a vortex. The length scale over which the order parameter recovers to the bulk value is a few times the coherence length (roughly, the size of a Cooper pair).

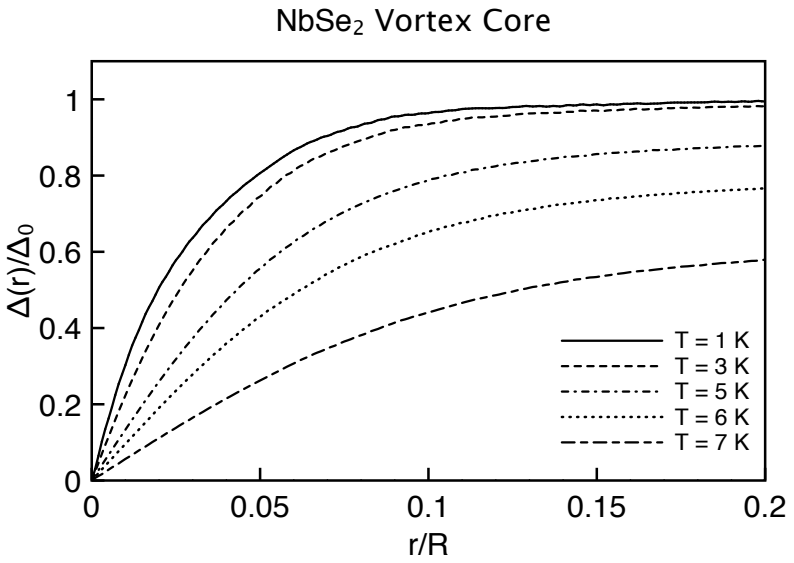

Figure 2.4: Converged order parameter around a vortex for various temperatures.

As introduced in Sec.1.3, the BdG equations are Schrödinger-like equations for the electron and hole amplitudes, u and v, of quasiparticle excitation and $\Delta(\vec{r})$ is a mean-field pairing potential that couples the electron and hole components. Around a vortex, the suppressed order parameter acts like a potential well to trap quasiparticles whose energies are smaller than the constant bulk value of the order parameter, i.e., the energy gap. This can be understood in terms of a square-well model for the order parameter around a vortex. In the normal region ($\Delta(\vec{r})$=0), an electron or a hole can exist; however, it cannot enter into the superconducting region ($\Delta(\vec{r}) \neq 0$) if its energy (measured from the Fermi energy) is smaller than the energy gap. However, an electron can enter into the superconducting region as a Cooper pair, taking along another electron (with opposite momentum and spin) with it. Then at the normal/superconductor interface, a hole is reflected back to the normal region. The hole, on the other hand, enters into the superconducting region at the opposite normal/superconductor interface as a hole Cooper pair, and thus an electron is reflected back. This is called the Andreev reflection [38]. In this way, a quasiparticle (a superposition of an electron and a hole) is trapped in the superconducting region. Such quasiparticle bound states are called Andreev

bound states [13, 14]. Similarly to the potential well problem in the normal state, such bound states exist with discrete energy levels, for which the electron and hole amplitudes interfere constructively.

For low temperature $T \lesssim 2$ K, the order parameter and the LDOS ($\frac{dI}{dV}$) are insensitive to temperature. We calculated the order parameter for $T = 0.1$ K and found it was almost the same as that for $T = 1$ K. For temperature $T \gtrsim 3$ K, as can be seen in Fig. 2.4, the order parameter is overall decreased with increasing temperature. The temperature dependence of the bulk value is consistent with Fig. 2.3. Temperature affects not only the value of the energy gap (the bulk order parameter), but also the radius of the "vortex core". The size of the vortex core decreases with decreasing temperature as can be seen in Fig. 2.4. The temperature dependence can be characterized by the vortex core size defined by [39]

$$\xi_c^{-1} = \lim_{r \to 0} \frac{\Delta(r)}{r} \frac{1}{\Delta(r = \infty)} \,. \tag{2.30}$$

As temperature is decreased, the slope of the order parameter at $r = 0$ increases and thus the core size decreases. In the limit of zero temperature, the slope diverges and the vortex core area shrinks to zero. This is called the Kramer-Pesch effect [39], and it stems from thermal depopulation of quasiparticle bound states in the core. When temperature decreases, the number of quasiparticles bound in the potential well decreases, which relieves suppression of the order parameter.

In Fig. 2.5, the energy eigenvalues are plotted as a function of angular momentum l for $T = 1$ K. It can be seen that a bound state branch (one bound state for each angular momentum that is smaller than a certain value) exists inside the energy gap. The bound state energy is almost zero for $l = 1/2$, and it approaches towards the gap edge as $|l|$ increases. The quantization (and the degeneracy) of energy levels in the scattering states is a finite-size effect due to finite radius R. However, the stronger quantization for small l, as can be seen in this figure, is due to resonance in the "potential well" region.

In Fig. 2.6, the electron and hole amplitudes of the lowest-energy bound state ($l = 1/2$) are shown ($T = 1$ K). It can be seen that the quasiparticle is confined in

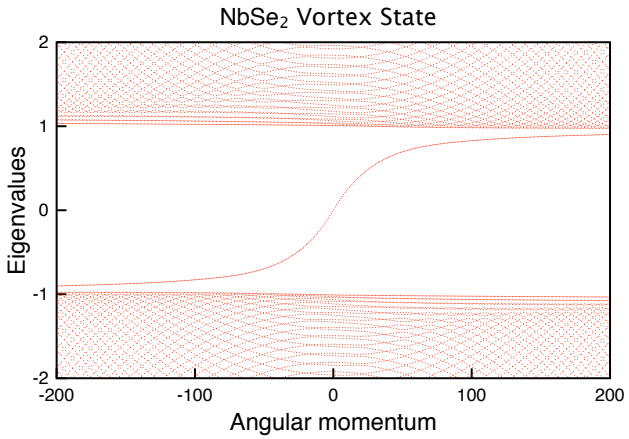

Figure 2.5: Energy levels of quasiparticle states as a function of angular momentum l.

the vortex core region, decaying rapidly for $r \gtrsim 0.1\,R$. It can also be seen that there is a phase shift between the electron and hole amplitudes. This is in contrast to the wavefunctions of scattering states, as illustrated in Fig. 2.7 for $l = 1/2$. One can see that in this case the wavefunction is extended outside the vortex core. As this is the lowest-energy scattering state, there is still a phase shift between the electron and hole amplitudes; however, the shift is only in the vortex core region.

Figure 2.8 shows the calculated dI/dV as a function of energy eV and radial distance r for $T = 1$ K. At $r = 0$, we can see the zero-energy bound state corresponding to $l = 1/2$. As one moves away from the vortex center, the bound state branches of positive energy (positive l) and negative energy (negative l) show up, merging finally to the gap edge, corresponding to large l. Far away from the vortex core, a coherence peak develops at the gap edge and the BCS DOS (dI/dV) is recovered. It is interesting to note that the "recovery length" over which the LDOS (dI/dV) recovers to the bulk behavior is substantially larger than that of the order parameter (see Fig. 2.4). The decay of the zero-bias peak as a function of r is consistent with that of the wavefunctions shown in Fig. 2.6.

The splitting of the zero-bias bound state peak for nonzero r can be seen clearly in the slices of dI/dV at various r shown in Fig. 2.9. It can be seen in this figure that at $r = 2000$ a.u. ($r/R = 0.2$) the bound state peak has almost merged to the

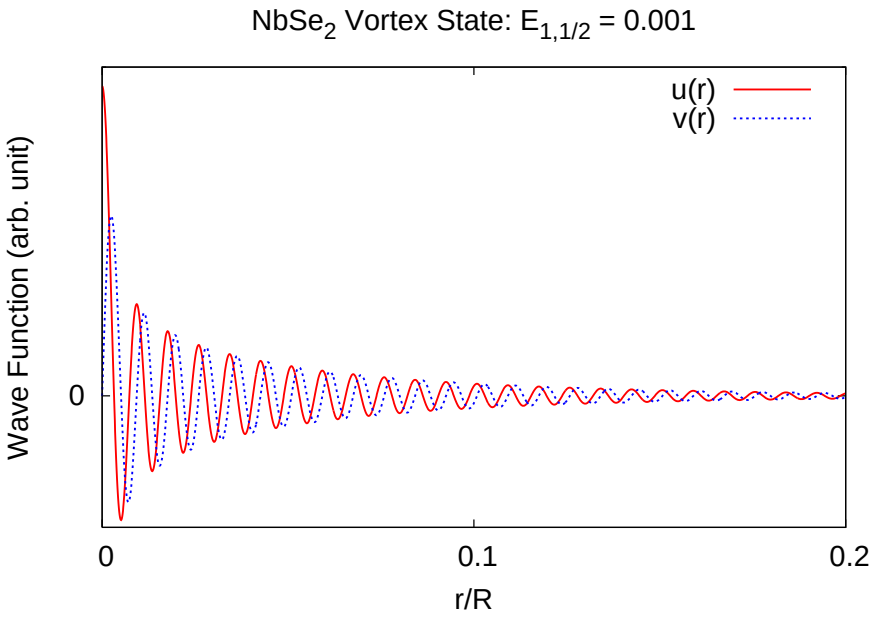

Figure 2.6: Electron and hole amplitudes of the quasiparticle bound state around a vortex for $l = 1/2$ and $T = 1$ K.

gap edge, where the coherence peak has started developing. However, this is still not quite the BCS behavior and one must go further away to recover the BCS DOS. The small oscillations for energies larger than the energy gap are due to the quantization of the energy levels described earlier.

Quasiparticle excitations around the vortex can be probed by tunneling an electron or a hole into the vortex core region by STM. In Fig. 2.10, the measured dI/dV as a function of radial distance and applied voltage at $T = 0.3$ K is shown. We can see that our result, Fig. 2.8, is consistent with the observation. In actual experiment, there are nonmagnetic impurities and defects in samples. They, along with finite temperature, tend to make dI/dV smeared compared with theoretical calculation. The excellent agreement with the experiment justifies our approximation of neglecting the spatial variation of magnetic field around a vortex. Our results are also consistent with those of GS [26] and it confirms the accuracy of our BdG program.

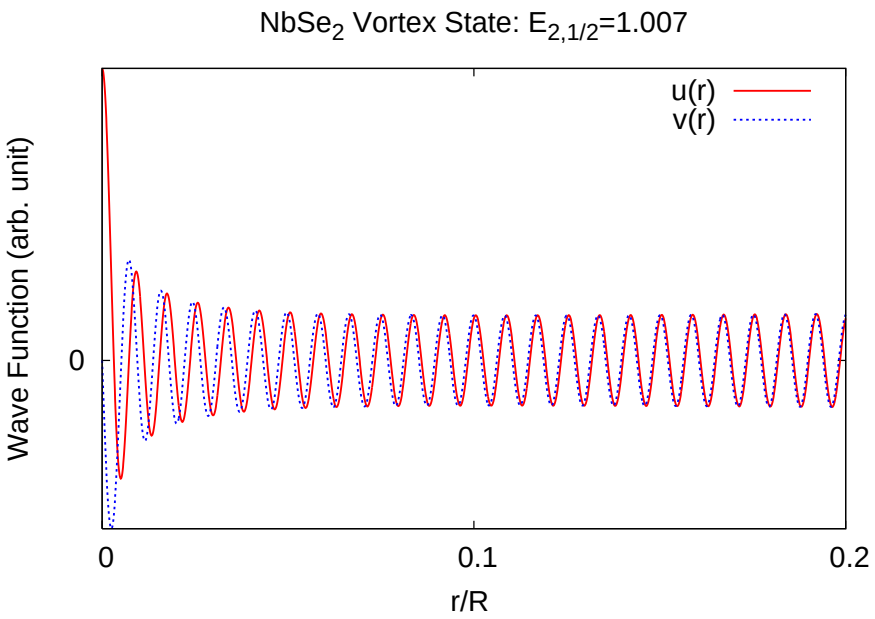

Figure 2.7: Electron and hole amplitudes of the lowest-energy scattering state around a vortex.

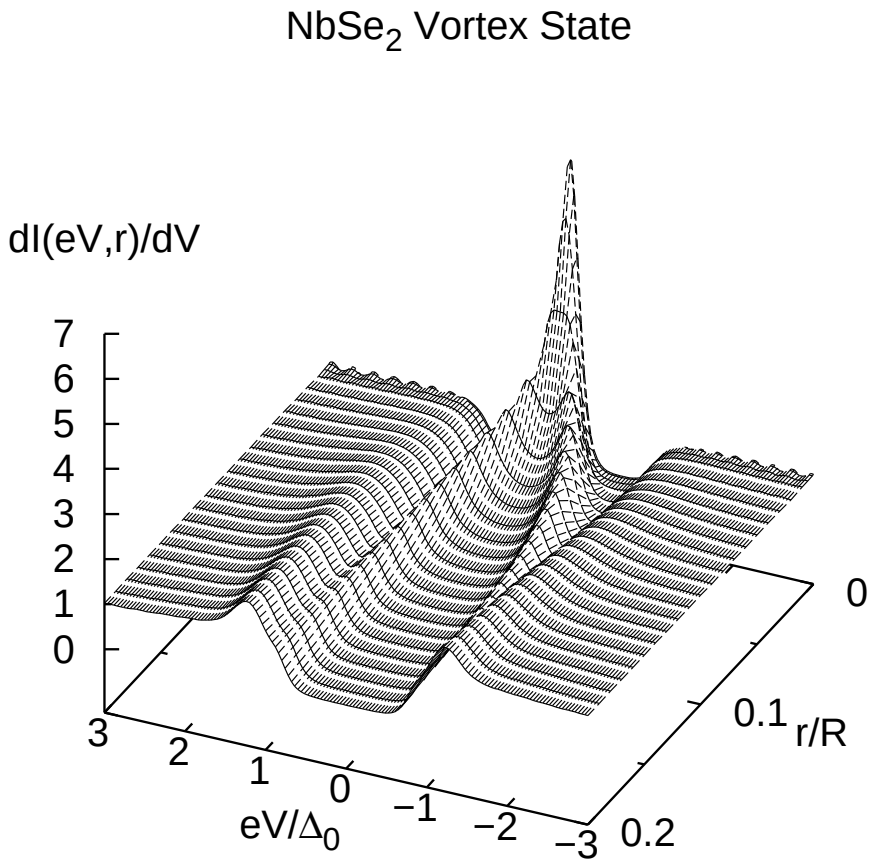

Figure 2.8: Tunneling conductance around a vortex for $T = 1$ K.

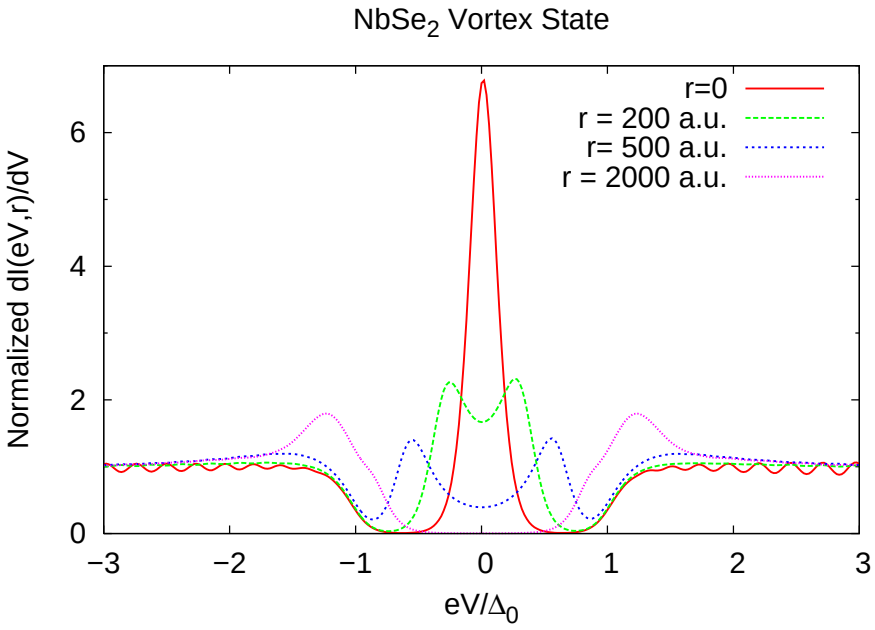

Figure 2.9: Tunneling conductance at various distances from the vortex center, obtained from Fig. 2.8.

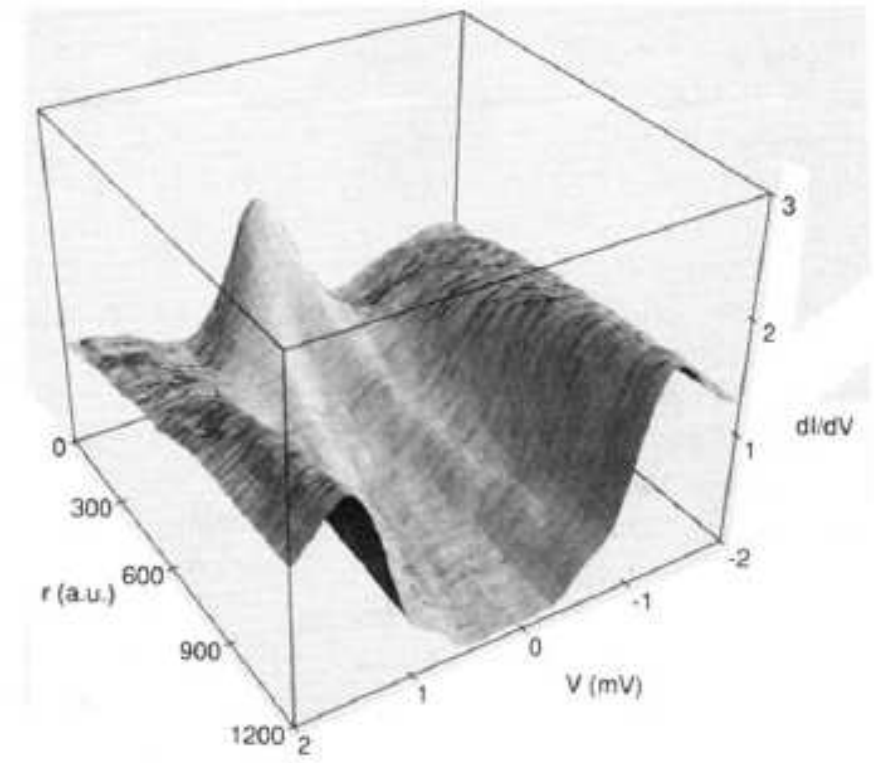

Figure 2.10: Tunneling conductance measured around a vortex in $NbSe_2$ at $T = 0.3$ K by Hess *et al.* [26].

Chapter 3

Electronic Structure around a Magnetic Impurity

In this chapter, electronic structure around an isolated magnetic impurity in an s-wave superconductor is examined within the framework of the BdG theory. The aim is to understand the pair-breaking nature of a magnetic impurity and the experimental observation of Ref. [20]. Magnetic impurity atoms tend to have the spins of neighboring electrons aligned or anti-aligned with their spin to form a net local magnetic moment, so that original Cooper pairs $(\vec{k}\uparrow, -\vec{k}\downarrow)$ are broken and thus superconductivity is suppressed locally. Similarly to a vortex, such a local magnetic moment results in inhomogeneous order parameter. Like the vortex problem, such inhomogeneity effects should be studied by solving the BdG equations selfconsistently. We model the interaction between the magnetic atom and the conduction electrons by a coupling of classical spins (i.e., we ignore dynamical effects) over the length scale of a few atomic distances. We assume that the spin potential created by the magnetic atom is spherical and solve the BdG equations in three-dimensional spherical coordinates.

In Sec.3.1, to check the three-dimensional program, the problem of a homogeneous superconductor is solved. In Sec.3.2, by assuming the spin potential to have a Gaussian form, we investigate the effects of a magnetic impurity.

3.1 Homogeneous System

3.1.1 Formulation

As discussed in the Sec.2.3, the order parameter $\Delta(\vec{r}) = \Delta(r) \equiv \Delta$ is a constant in a homegenous system. With spherical symmetry, radial and angular coordinates, (r, θ, ϕ), of the quasiparticle wavefunctions can be separated as

$$\begin{aligned} u_n(\vec{r}) &= u_{\nu,l}(r) Y_{l,m}(\theta, \phi) \ , \\ v_n(\vec{r}) &= v_{\nu,l}(r) Y_{l,m}(\theta, \phi) \ , \end{aligned} \tag{3.1}$$

where $\{Y_{l,m}; l = 0, 1, 2, \cdots ; m = -l, \cdots , l\}$ are the spherical harmonics:

$$Y_{l,m}(\theta, \phi) = (-1)^m \sqrt{\frac{2l+1}{4\pi} \frac{(l-m)!}{(l+m)!}} P_l^m(\cos\theta) \mathrm{e}^{\mathrm{i}m\phi} \, . \tag{3.2}$$

The ν above is the nodal quantum number (ν = 1,2,$\cdots$). Using Eqs. (3.1), the BdG equations can be reduced to

$$\begin{pmatrix} \hat{H}_r & \Delta \\ \Delta & -\hat{H}_r^\star \end{pmatrix} \begin{pmatrix} u_{\nu,l}(r) \\ v_{\nu,l}(r) \end{pmatrix} = E_{\nu,l} \begin{pmatrix} u_{\nu,l}(r) \\ v_{\nu,l}(r) \end{pmatrix} , \tag{3.3}$$

where $\hat{H}_r = -\frac{\hbar^2}{2m} \left[\frac{d^2}{dr^2} + \frac{2}{r} \frac{d}{dr} + \frac{l(l+1)}{r^2} \right] - E_F$. Analogously to the method for the vortex problem, the radial wavefunctions can be expanded in terms of the complete orthonormal set of the spherical Bessel functions:

$$\begin{aligned} u_{\nu,l}(r) &= \sum_k c_{\nu,k} \rho_{k,l}(r) \, , \\ v_{\nu,l}(r) &= \sum_k d_{\nu,k} \rho_{k,l}(r) \, , \end{aligned} \tag{3.4}$$

where

$$\begin{aligned} \rho_{k,l}(r) &= \frac{\sqrt{2}}{\sqrt{R^3}} j_l(\alpha_{k,l} \frac{r}{R}) / j_{l+1}(\alpha_{k,l}) \\ &= \frac{\sqrt{2}}{R\sqrt{r}} J_{l+\frac{1}{2}}(\alpha_{k,l} \frac{r}{R}) / J_{l+\frac{3}{2}}(\alpha_{k,l}) \, . \end{aligned} \tag{3.5}$$

Here the spherical Bessel functions of order l, $j_l(\alpha_{k,l}\frac{r}{R})$, are normalized in a sphere of radius R and $\alpha_{k,l}$ is the k-th zero of j_l. The $J_{l+\frac{1}{2}}$ is the cylindrical Bessel function with a fractional order $l+\frac{1}{2}$:

$$j_l(x) = \sqrt{\frac{\pi}{2x}} J_{l+\frac{1}{2}}(x).$$

As in the vortex problem, in a weak-coupling superconductor, only those states close to the Fermi surface are relevant to superconductivity. We consider only the states with energy below $E_F + \epsilon$, where ϵ is of the order of $\hbar\omega_D$. The maximum nodal quantum number N_l for a given l is determined by

$$\frac{\hbar^2 \alpha_{N_l l}^2}{2mR^2} \leq E_F + \epsilon. \tag{3.6}$$

Substituting Eq. (3.4) into Eq. (3.3), we obtain a $2N_l \times 2N_l$ matrix equation for the expansion coefficients for each angular momentum l:

$$\begin{pmatrix} T & \widetilde{\Delta} \\ \widetilde{\Delta} & -T \end{pmatrix} \psi_{\nu,l} = E_{\nu,l} \psi_{\nu,l}\,, \tag{3.7}$$

where $\psi_{\nu,l}^T = (c_{k,1}, \cdots, c_{k,N_l}, d_{k1}, \cdots, d_{kN_l})$. The equation has $2N_l$ sets of eigenvalues E_ν and eigenvectors ψ_ν. Due to orthonormality of the Bessel functions, matrix elements of the Hamiltonian are given by

$$\begin{aligned} T_{k,k'} &= \langle k, l | \hat{H}_r | k', l \rangle \\ &= \left(\frac{\hbar^2 \alpha_{k,l}^2}{2m} - E_F \right) \delta_{k,k'} \end{aligned} \tag{3.8}$$

and

$$\widetilde{\Delta}_{k,k'} = \langle k, l | \Delta | k', l \rangle = \Delta \delta_{k,k'}\,. \tag{3.9}$$

In the gap equation,

$$\Delta(\vec{r}) = g \sum_{0 \leq E_{\nu,l,m} \leq \hbar\omega_D} u_{\nu,l,m}(\vec{r}) v^\star_{\nu,l,m}(\vec{r}) [1 - 2f(E_{\nu,l,m})], \tag{3.10}$$

the summation is over the three quantum numbers, $n = (\nu, l, m)$. The order parameter in a spherically symmetric system should be a function of radial coordinate only.

One can see this by substituting Eq. (3.1) into Eq. (3.10) and using the following property of the spherical harmonics [40].

$$\sum_{m=-l}^{l} Y_{l,m} Y_{l,m}^{\star} \propto 2l+1 \ .$$

Thus

$$\Delta(\vec{r}) \propto g \sum_{0 \le E_{\nu,l} \le \hbar\omega_D} u_{\nu,l}(r) v_{\nu,l}(r)^{\star} \Big[1 - 2f(E_{\nu,l}) \Big] (2l+1).$$

Similarly, we have:

$$A(\vec{r}, E) \propto \sum_{\nu,l} [|u_{\nu,l}(r)|^2 \delta(E - E_{\nu,l}) + |v_{\nu,l}(r)|^2 \delta(E + E_{\nu,l})](2l+1), \tag{3.11}$$

$$\frac{\partial I(\vec{r}, V)}{\partial V} \propto -\sum_{\nu,l} [|u_{\nu,l}(r)|^2 f'(E_{\nu,l} - eV) + |v_{\nu,l}(r)|^2 f'(E_{\nu,l} + eV)](2l+1). \tag{3.12}$$

3.1.2 Results and Discussion

The program for the three-dimensional BdG equations has first been applied to the homogeneous problem. In Fig. 3.1, the tunneling conductance, dI/dV for clean Nb for $T = 1$ K is shown. For Nb, $E_F = 950$ meV, the zero-temperature gap Δ_0 =1.45 meV, $\hbar\omega_D$ =23.86 meV, and T_c=9.2 K. The result shown is for the system size R =15,000 a.u.. The LDOS (e.g., with smoothing width γ=0.1) looks very similar to dI/dV. As can be seen in Fig. 3.1, dI/dV clearly shows the energy gap and the coherence peak, and as expected, it is independent of position r. The oscillations in dI/dV outside the energy gap are a finite-size effect due to finite R. In three dimensions, quantization of the energy levels is more pronounced than in two dimensions presented in Chapter 2.

3.2 Isolated Magnetic Impurity

3.2.1 Formulation

The problem of magnetic exchange interactions between a magnetic impurity atom and the conduction electrons is very complex. There are several models with different

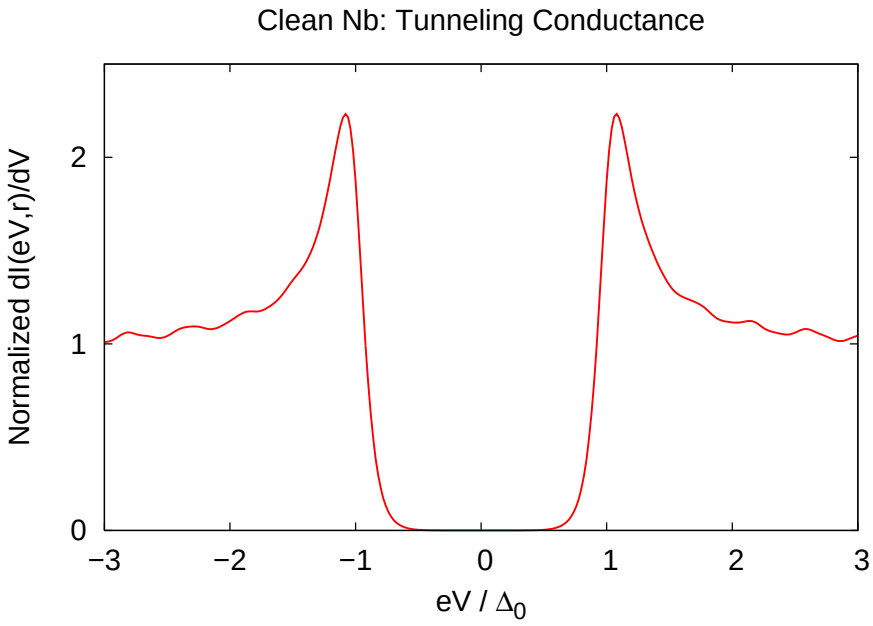

Figure 3.1: Tunneling conductance of a pure Nb at temperature T=1 K.

levels of approximations to deal with this problem. One method [41] assumes the exchange interaction to be isotropic, taking into account of screening effects of the Coulomb interaction. The Hamiltonian can be written as

$$H_{at} = -2J_{at}\vec{S}\cdot\vec{s},$$

where $\vec{S}$ is the spin of the magnetic impurity and $\vec{s}$ is the conduction electron spin at the position of the magnetic impurity. The J_{at} signifies the coupling strength between the spins and it is always positive [41]. At this level, we neglect effects of the covalent mixing which means that local orbitals of the magnetic impurity form covalent bonds with the conduction electrons. To incorporate the covalent mixing into the equation above, Schrieffer and Wolff [42] have shown that J_{at} should be replaced with a generalized J, where

$$H = -2J\vec{S}\cdot\vec{s},$$

and

$$J = J_{at} + J_{cm}\,.$$

The J_{cm} represents the strength of covalent mixing and it can be positive or negative, depending on the orbital nature of the conduction electrons [43]. Weights of the two

components determine the sign of J. The magnetic impurity with $J > 0$ ($J < 0$) is ferromagnetic (antiferromagnetic). Mn and Gd, the two magnetic atoms used in the experiment of Yazdani *et al.*, are common choices for studying their magnetic properties experimentally. Both of them can be ferromagnetic or antiferromagnetic depending on the host. For Mn, J_{cm} is usually negative and even dominates J_{at} [41]. But exceptions still exist. For example, J is positive in MgB_2 [44]. For Gd, J is positive in the superconducting materials La and $LaAl_2$ [45], and it is negative in another superconducting material $LaOs_2$ [43].

In the model above, dynamical effects of magnetic interactions can be included by introducing an additional field at the impurity site [43]. However, in a fully-gapped s-wave superconductor, we can assume the spin of the magnetic impurity to be classical and static [20, 46]. Therefore, in our work, we introduce a spin-dependent static potential provided by the magnetic impurity to model its spin effects on the conduction electrons. The effective Hamiltonian Eq. (1.20) is generalized as

$$\begin{aligned}\hat{H}_{eff} = \int d\vec{r}\Big[&\Psi_\uparrow^\dagger(\vec{r})\hat{H}_e(\vec{r})\Psi_\uparrow(\vec{r}) + \Psi_\downarrow^\dagger(\vec{r})\hat{H}_e(\vec{r})\Psi_\downarrow(\vec{r}) \\ &- U_{spin}(\vec{r})\Psi_\uparrow^\dagger(\vec{r})\Psi_\uparrow(\vec{r}) + U_{spin}(\vec{r})\Psi_\downarrow^\dagger(\vec{r})\Psi_\downarrow(\vec{r}) \\ &+ \Delta(\vec{r})\Psi_\uparrow^\dagger(\vec{r})\Psi_\downarrow^\dagger(\vec{r}) + \Delta^\star(\vec{r})\Psi_\downarrow(\vec{r})\Psi_\uparrow(\vec{r})\Big]. \quad (3.13)\end{aligned}$$

The third and the fourth terms are the potential energies of spin-up and spin-down electrons, respectively. Furthermore, this potential is assumed to be spherically symmetric and of a Gaussian form,

$$U_{spin}(\vec{r}) \equiv V_s \exp\left[-\left(\frac{r}{\lambda}\right)^2\right], \quad (3.14)$$

where λ is a length scale of the spin potential and V_s represents the coupling strength. This is a good approximation for Mn, which has three valence electrons. When $V_s > 0$ ($V_s < 0$), the coupling is ferromagnetic (antiferromagnetic). Assuming the coupling is ferromagnetic, this potential decreases the energy of an electron with spin up (a hole with spin down) and increases that of an electron with spin down (a hole with

spin up). Starting from this effective Hamiltonian, we can derive the BdG equations:

$$\begin{pmatrix} \hat{H}_e - U_{spin} & \Delta(\vec{r}) \\ \Delta(\vec{r}) & -\hat{H}_e^\star - U_{spin} \end{pmatrix} \begin{pmatrix} u_{n,\uparrow}(\vec{r}) \\ v_{n,\downarrow}(\vec{r}) \end{pmatrix} = E_{n\uparrow} \begin{pmatrix} u_{n,\uparrow}(\vec{r}) \\ v_{n,\downarrow}(\vec{r}) \end{pmatrix}, \tag{3.15}$$

and

$$\begin{pmatrix} \hat{H}_e + U_{spin} & \Delta(\vec{r}) \\ \Delta(\vec{r}) & -\hat{H}_e^\star + U_{spin} \end{pmatrix} \begin{pmatrix} u_{n,\downarrow}(\vec{r}) \\ v_{n,\uparrow}(\vec{r}) \end{pmatrix} = E_{n\downarrow} \begin{pmatrix} u_{n,\downarrow}(\vec{r}) \\ v_{n,\uparrow}(\vec{r}) \end{pmatrix}. \tag{3.16}$$

If the coupling is antiferromagnetic, the sign of U_{spin} is reversed; however, the combination of the two BdG equations above give the same result as for ferromagnetic coupling. A spin-up (-down) bound state is a superposition of a spin-up (-down) electron and a spin-down (-up) hole. One can obtain the results of the equations for spin-down states Eq. (3.16) from those for spin-up states Eq. (3.15), by the transformation,

$$\begin{aligned} u_{n\uparrow} &= -v_{n\uparrow}\,, \\ v_{n\downarrow} &= u_{n\downarrow}\,, \\ E_{n\uparrow} &= -E_{n\downarrow}\,. \end{aligned} \tag{3.17}$$

Therefore, we only have to solve Eq. (3.15) for positive- and negative-energy states, and obtain the solutions of Eq. (3.16) through these relations.

As in the homogeneous problem, the quasiparticle wavefunctions can be taken apart into radial and angular parts. The radial BdG equations are

$$\begin{pmatrix} \hat{H}_r - U_{spin} & \Delta(r) \\ \Delta(r) & -\hat{H}_r^\star - U_{spin} \end{pmatrix} \begin{pmatrix} u_{\nu,l,\uparrow}(r) \\ v_{\nu,l,\downarrow}(r) \end{pmatrix} = E_{\nu,l,\uparrow} \begin{pmatrix} u_{\nu,l,\uparrow}(r) \\ v_{\nu,l,\downarrow}(r) \end{pmatrix}, \tag{3.18}$$

where $\hat{H}_r = -\frac{\hbar^2}{2m}\left[\frac{d^2}{dr^2} + \frac{2}{r}\frac{d}{dr} + \frac{l(l+1)}{r^2}\right] - E_F$. Here the pairing potential Δ is only a function of distance r due to the spherical symmetry of the impurity potential. As before, we expand the radial wavefunctions in terms of the complete orthonormal set of the spherical Bessel functions $\{j_l(x)\}$. For relatively strong spin potential, states far away from the Fermi surface can be affected. Thus much more states are included in the gap equation compared with the vortex problem. The matrix

equation for each l is

$$\begin{pmatrix} T-\widetilde{U} & \widetilde{\Delta} \\ \widetilde{\Delta} & -T-\widetilde{U} \end{pmatrix} \psi_{\nu,l,\uparrow} = E_{\nu,l,\uparrow}\psi_{\nu,l,\uparrow}\,, \tag{3.19}$$

where $\psi^T_{\nu,l,\uparrow} = (c_{k,1}, \cdots, c_{k,N_l}, d_{k,1}, ..., d_{k,N_l})$, and

$$\begin{aligned} T_{k,k'} &= \langle k,l|\hat{H}_r|k',l\rangle \\ &= \left(\frac{\hbar^2\alpha^2_{k,l}}{2m} - E_F\right)\delta_{k,k'}, \\ \widetilde{\Delta}_{k,k'} &= \langle k,l|\Delta(r)|k',l\rangle \\ &= \int_0^\infty \rho_{k,l}(r)\Delta(r)\rho_{k',l}(r)r^2dr \\ \widetilde{U}_{k,k'} &= \langle k,l|U(r)|k',l\rangle \\ &= V_s\int_0^\infty r^2\rho_{k,l}(r)\rho_{k',l}(r)\exp\left[-\left(\frac{r}{\lambda}\right)^2\right]\mathrm{d}r. \end{aligned} \tag{3.20}$$

Here again we utilize parallel computation, following the flow chart in Fig. A.4 and assigning different sets of l values to different nodes. The numerical procedure is discussed in Sec. A.3.4 . As in the vortex problem, curve fitting (Appendix B) is used for evaluation of the matrix elements.

3.2.2 Results and Discussion

As discussed in the Appendix, the major difficulty in computation for Nb exists in the integration of matrix elements $\langle k,l|\Delta(r)|k',l\rangle$. The larger the nodal number k, the more oscillations the Bessel functions have, and this makes the numerical calculation challenging. The maximum nodal number N_l is determined by Eq. (2.7), namely, $N_l^2 \propto (E_F+\epsilon)R^2$. Due to very large E_F (≈ 950 meV) for Nb, we have been able to solve the BdG equations for $R \leq 3,000$ a.u.. However, we have another numerical problem in this case. The difference between two neighboring energies for a given l, $E_{\nu,l}$ and $E_{\nu+1,l}$, can be roughly estimated by

$$
\begin{aligned}
E_{\nu,l} - E_{\nu+1,l} &\approx \frac{\hbar^2}{2mR^2}(\alpha_{k,l}^2 - \alpha_{k+1,l}^2), \\
&\approx \frac{\hbar^2}{2mR^2}(-2 * \pi\alpha_{k,l}), \qquad \text{assuming } \alpha_{k,l} + \pi \approx \alpha_{k+1,l}\,, \\
&\qquad\qquad\qquad\qquad\qquad\qquad\qquad\qquad\qquad\qquad \alpha_{k,l} \gg \pi\,, \\
&\approx -\frac{\sqrt{2}\pi\hbar}{\sqrt{m}}\frac{\sqrt{E_{\nu,l}}}{R}.
\end{aligned}
$$

Thus large E_F ($\approx E_{\nu,l}$) and small R lead to strong quantization of energy levels. The quantization may be so large that the tunneling conductance has only isolated peaks even in continuum. This may make that distinction of possible bound states from continuum states difficult. Thus to study the effects of a magnetic impurity, we perform a model calculation with parameter values which yield less energy quantization. Analogously to parameters of $NbSe_2$, we model a superconductor with $E_F = 40$ meV, Δ_0 =1.2 meV and T =1 K. The coupling constant g is about 111 meV·Å for R =8,000 a.u. and $\hbar\omega_D$ =3 meV. We present results for ferromagnetic coupling only. We have confirmed that antiferromagnetic coupling (reversing the sign of V_s) gives the same results, as mentioned in the last section. The length scale λ of the spin potential $U_{spin}(r)$ is taken to be 10 a.u., while the strength V_s is varied from 100 meV to 4 eV.

Figure 3.2 shows the converged order parameter $\Delta(r)$ as a function of r for several values of V_s. Similarly to the order parameter in the vortex problem in Fig. 2.4, it is suppressed around the impurity and recovers to the bulk value as r increases. As discussed above, such suppression of the order parameter indicates that Cooper pairs are broken and superconductivity is suppressed around a magnetic impurity. Unlike the vortex problem, however, the order parameter at the impurity site, $\Delta(r = 0)$, is not necessarily zero, depending on the potential strength V_s. As can be seen in Fig. 3.2, for a relatively small V_s, $\Delta(r)$ is only weakly suppressed and $\Delta(r = 0) > 0$. As V_s increases, $\Delta(r = 0)$ is reduced further. For V_s beyond a certain critical value $V_c \approx 915.8$ meV, it becomes negative. Interestingly, as V_s is increased further, at some point, $V_c' \approx 1150$ meV, $\Delta(r = 0)$ starts increasing towards zero (though stays

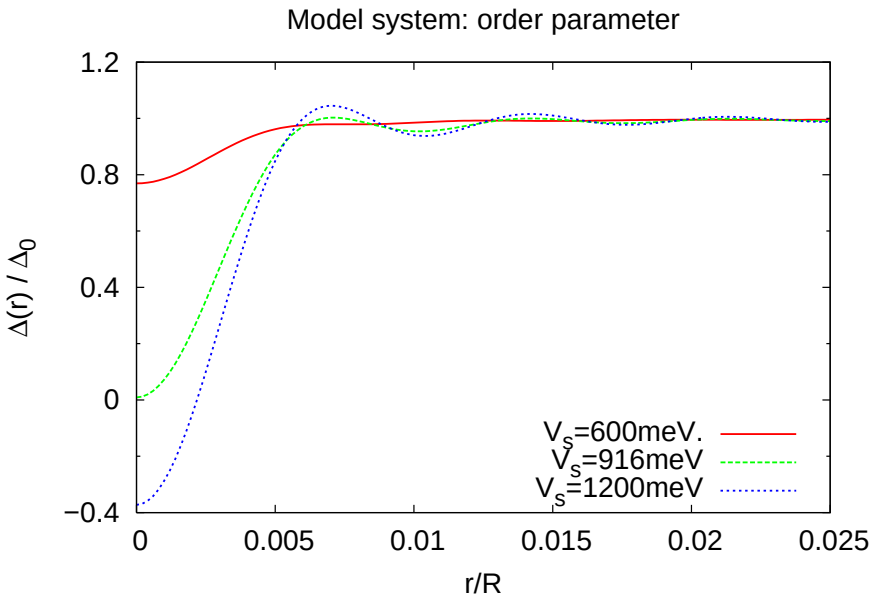

Figure 3.2: Order parameter around a magnetic impurity for different strengths of the spin potential.

negative). This behavior is illustrated in Fig. 3.3, where $\Delta(r=0)$ (red solid curve) and $|\Delta(r=0)|$ (green dashed curve) are plotted as a function of V_s. As mentioned before, $\Delta(r)$ corresponds to the Copper pair wavefunction in the macroscopic picture. The $|\Delta(r=0)|$ signifies the strength of superconductivity at $r=0$. It can be seen in Fig. 3.3 that, as V_s increases, superconductivity is suppressed to zero at $V_s = V_c$, and then it is practically restored for $V_c < V_s < V_c'$, and then it is suppressed again towards zero as V_s goes to infinity.

We plot bound state energies as a function of V_s in Fig. 3.4. There are 4 branches shown in this figure. The red and green curves are spin-up and spin-down bound states from Eqs. (3.15) and Eqs. (3.16), respectively, for $l=0$. As V_s increases, both branches move from the gap edge towards the Fermi energy and then towards the gap edge on the other side. A bound state with positive energy ($E_n = E > 0$) means that an electron can be tunneled into the superconductor when a positive bias voltage is applied, and the energy of the quasiparticle excitation is E. A bound state with negative energy ($E_n = -E < 0$) means that an electron can be tunneled out when a negative bias voltage is applied, and the energy of the quasiparticle excitation is also E. For relatively weak spin potential ($V_s < V_c$), an electron with spin down can

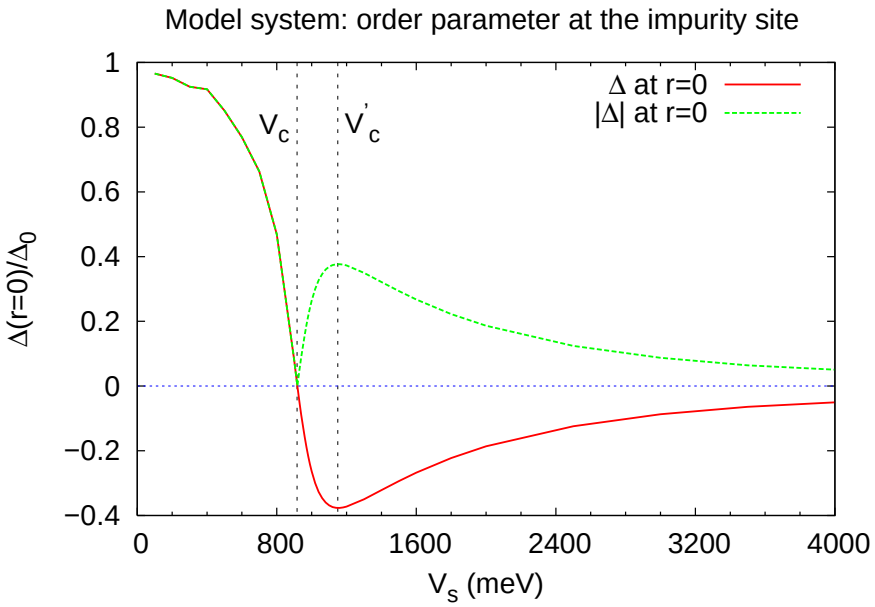

Figure 3.3: Order parameter at $r = 0$ as a function of the spin potential strength V_s. The critical values V_c and V_c' are indicated.

be tunneled out and a hole with spin up is left and bound to the magnetic impurity (ferromagnetic coupling). The resulting spin-up quasiparticle suppresses $\Delta(r = 0)$ and superconductivity. When V_s becomes larger than V_c, a quasiparticle with spin up is bound to the impurity in the *ground state*. By applying negative bias, one can remove this quasiparticle from the impurity site. By applying positive bias, one can tunnel an electron with spin down into the superconductor, and this electron can form a Cooper pair with the spin-up electron bound to the impurity and the Cooper pair goes into the condensation. This restores $\Delta(r = 0)$ and superconductivity.

For the range of potential strength shown in Fig. 3.4, l =0 bound states are dominant; however, as V_s increases further, l =1 bound states appear and would behave similarly as the l =0 bound states as a function of V_s for much larger V_s. However, for a physically reasonable value of V_s as shown in Fig. 3.4, l =1 bound states do not have significant contribution, due to the short range ($\lambda = 10$ a.u.) of the potential.

In Fig. 3.5, we present the electron and hole amplitudes, $u_\uparrow(r)$ and $v_\downarrow(r)$, of the l =0 bound state as a function of r, for V_s =600 meV. As can be seen in this figure, the wavefunction decays rapidly as r increases and the quasiparticle is bound

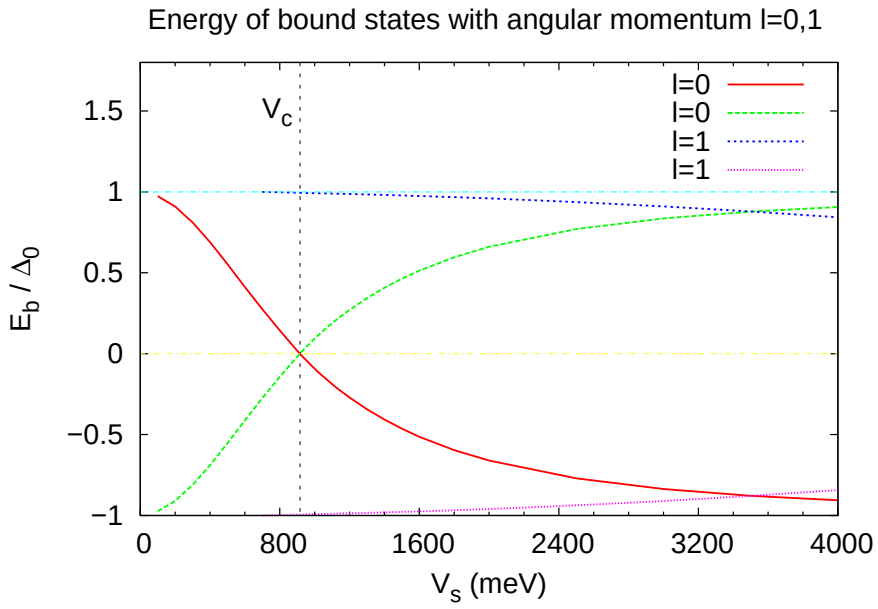

Figure 3.4: Energies of the bound states with the angular momentum $l = 0, 1$ as a function of the spin potential strength.

within the region where the order parameter is suppressed (see Fig. 3.2). There is always a phase shift between the electron and hole components of a bound state. Figure 3.6 shows the electron and hole amplitudes for a scattering state for l =0 and $V_s = 600$ meV. The scattering states extend outside "the potential well" and there is a phase shift between the two components only very close to the impurity site, which disappears quickly as r increases.

In Fig. 3.7, the phase shift between the electron and hole components of a spin-up bound state is plotted as a function of V_s. It can be seen that the phase shift increases as V_s increases and approaches π in the limit that V_s is very large. The phase shift is about $\pi/2$ at the critical value V_c where the sign of $\Delta(r = 0)$ changes from positive to negative and the energies of the spin-up and spin-down bound states are both zero. As a result of the phase shift between the electron and hole amplitudes, there is asymmetry between positive and negative energies in the LDOS (dI/dV). This is illustrated in Fig. 3.8, where the tunneling conductance at the impurity site ($r = 1$ a.u.) is plotted as a function of bias voltage for V_s =600, 916 and 1200 meV. When $V_s < V_c$ (V_s=600 meV), the peak in the tunneling conductance for positive bias is higher than that for negative bias. This means that the probability amplitude

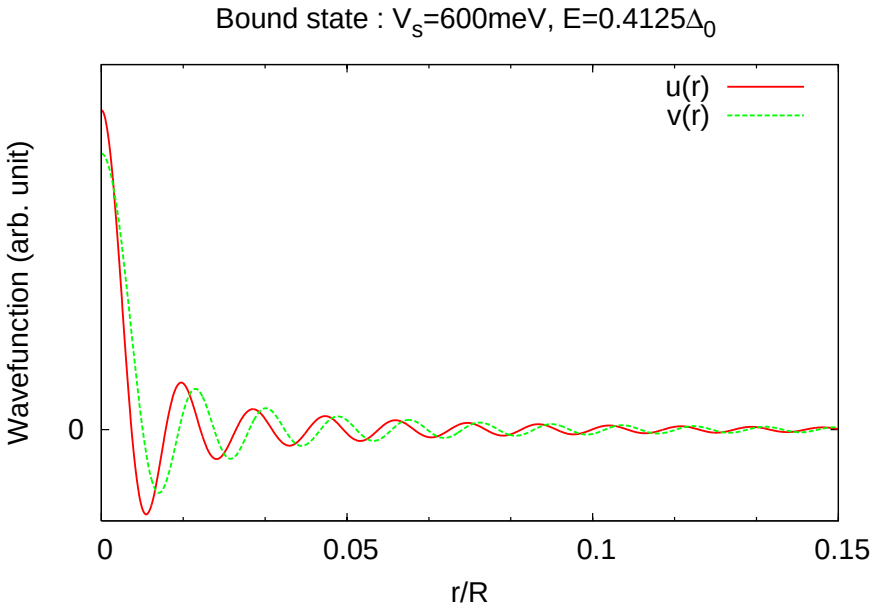

Figure 3.5: Electron and hole amplitudes of the $l = 0$ bound state.

of a spin-up quasiparticle excitation (tunneling an electron in with positive bias) is larger than that of a spin-down quasiparticle excitation (tunneling an electron out with negative bias). For $V_s > V_c$ (V_s=1200 meV), the asymmetry is opposite. As discussed above, in this case, a spin-up quasiparticle is bound to the impurity in *ground state* and the hole-like excitation is in favor instead. Such asymmetry in the tunneling conductance has been observed in the experiment of Yazdani *et al.*. They found particle-hole asymmetry in the tunneling conductance over the Mn atom similar to that for V_s =1200 meV in our model. On the other hand, opposite asymmetry was observed over Gd, as found for V_s =600 meV by our calculation. We thus propose, within the classical spin model, that the effective interaction strength between the magnetic impurity and the conduction electrons is different in these two materials, resulting in different natures of quasiparticle excitations. Changes of the nature of bound states as V_s varies are illustrated in Fig. 3.10 and Fig. 3.11, where dI/dV is plotted as a function of energy and the potential strength V_s. As seen in Fig. 3.10, bound states appear at the gap edge as V_s increases from zero. Then the magnitude of the bound state energies decreases as V_s increases, and at $V_s = V_c$, the two bound state peaks merge at zero energy. As V_s is increased further (Fig. 3.11), the zero-bias peak splits and the bound state peaks approach the gap edge. It can

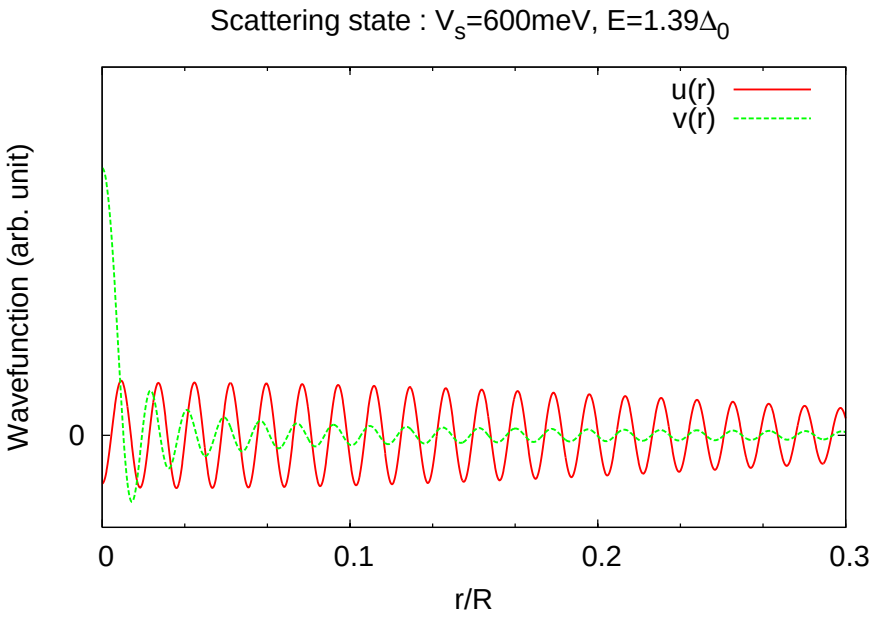

Figure 3.6: Electron and hole amplitudes of a $l = 0$ scattering state.

be seen in Fig. 3.11 that in this case, the negative energy bound state peak is always higher than the peak for positive energy.

Although the range of the spin potential λ is about 10 a.u., the wavefunction of a bound quasiparticle extends over a slightly larger region. This is illustrated in Fig. 3.12, where dI/dV at several positions is plotted as a function of bias voltage for $V_s = 916$ meV. The $V_s = 916$ meV is the critical potential strength that yields zero-energy bound states. The zero-bias peak is visible in Fig. 3.12 even at $r = 200$ a.u., while the coherence peak has developed at the gap edge. To investigate the spatial structure of the tunneling conductance further, dI/dV is plotted as a function of energy and distance r in Fig. 3.13 ($V_s = 916$ meV), Fig. 3.14 ($V_s = 600$ meV) and Fig. 3.15 ($V_s = 1200$ meV). For these values of V_s, the $l = 1$ bound states are almost at the gap edge and not visible in dI/dV due to thermal smearing. So we see the $l = 0$ bound states only. In all the three cases, the bound states inside the energy gap are discernible at distance r much larger than λ. On the other hand, as one moves away from the impurity, the coherence peak develops and the BCS density of states is recovered (except for the bound state peaks) at $r = 120$ a.u. more or less. Thus it is possible to probe quasiparticle bound states by STM a little way off the

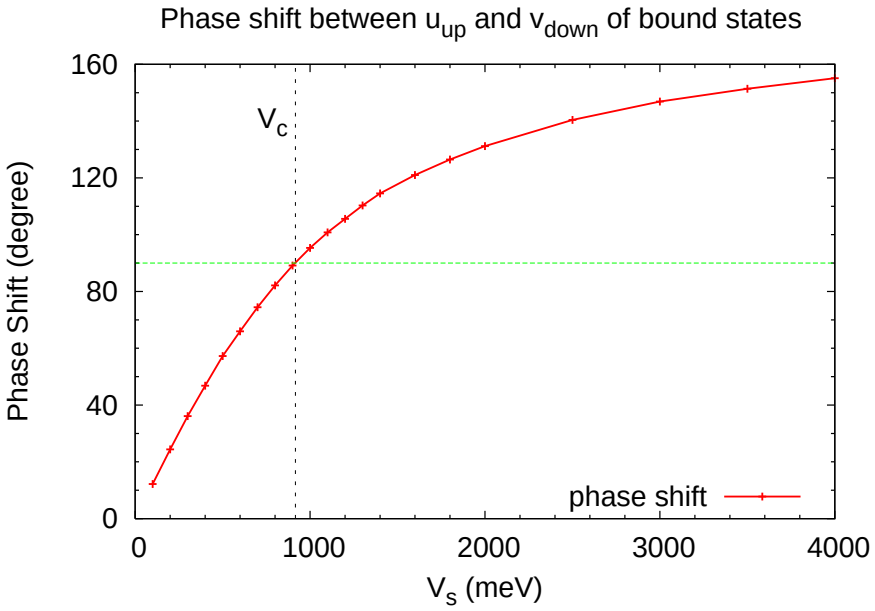

Figure 3.7: Phase shift between the electron and hole amplitudes of the spin-up bound state as a function of the spin potential strength V_s.

impurity site.

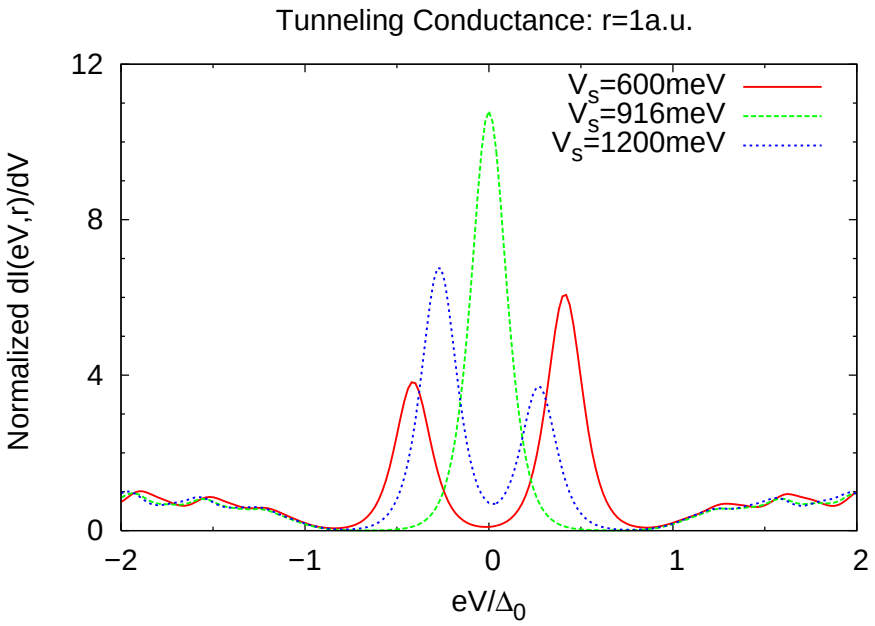

Figure 3.8: Tunneling conductance of as a function of bias voltage on top of the magnetic impurity, for three different values of potential strength V_s.

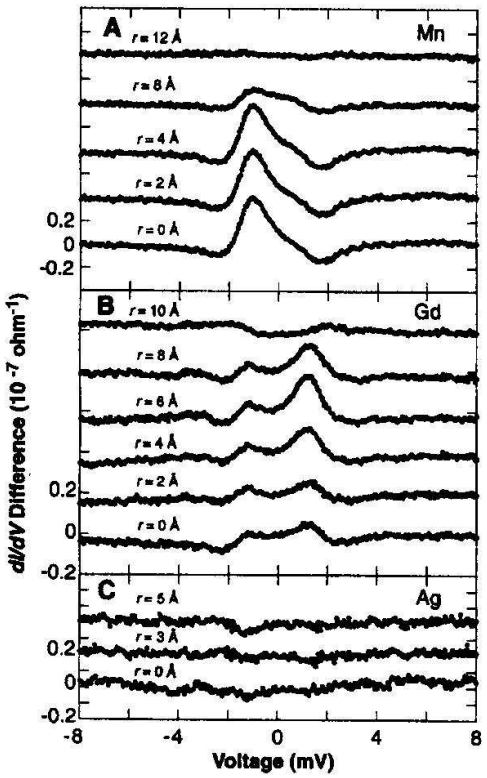

Figure 3.9: Difference spectra measured near isolated (A) Mn, (B) Gd, and (C) Ag atom [20].

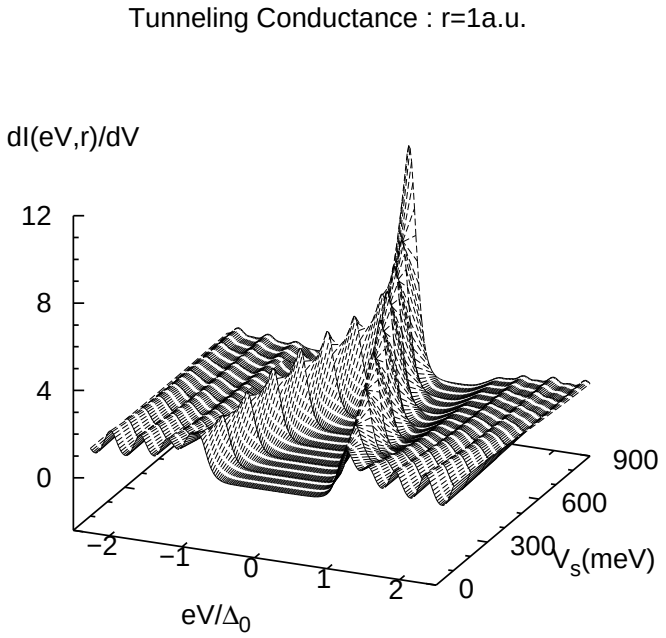

Figure 3.10: Tunneling conductance on top of the magnetic impurity as a function of bias voltage and spin potential strength V_s.

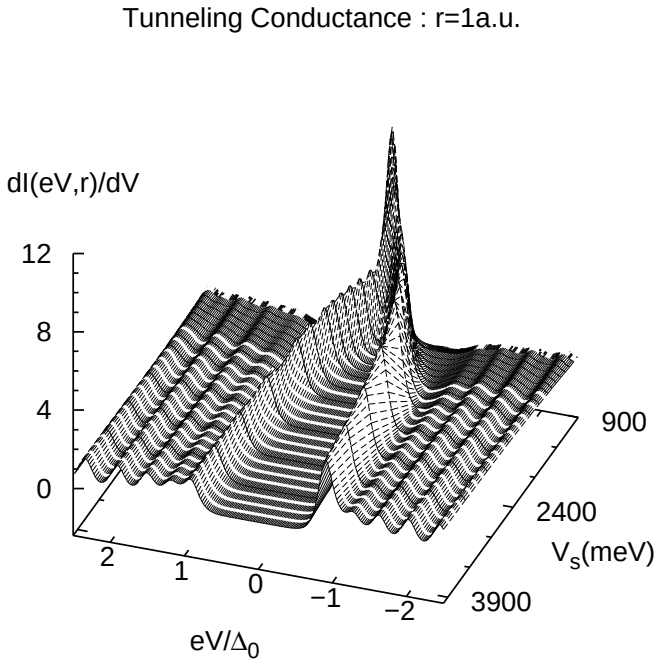

Figure 3.11: Same as Fig. 3.10 but for larger V_s.

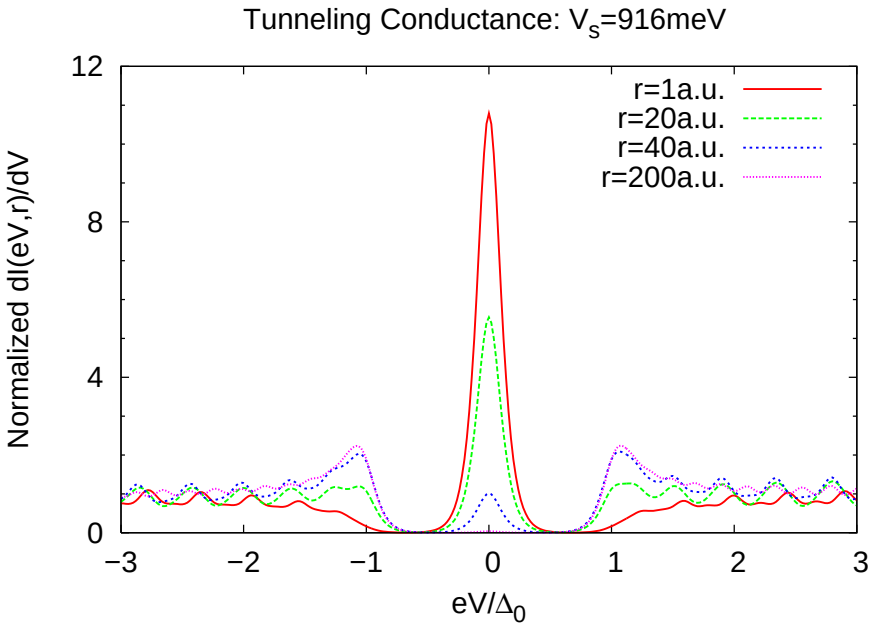

Figure 3.12: Tunneling conductance as a function of energy eV at different radial distances r.

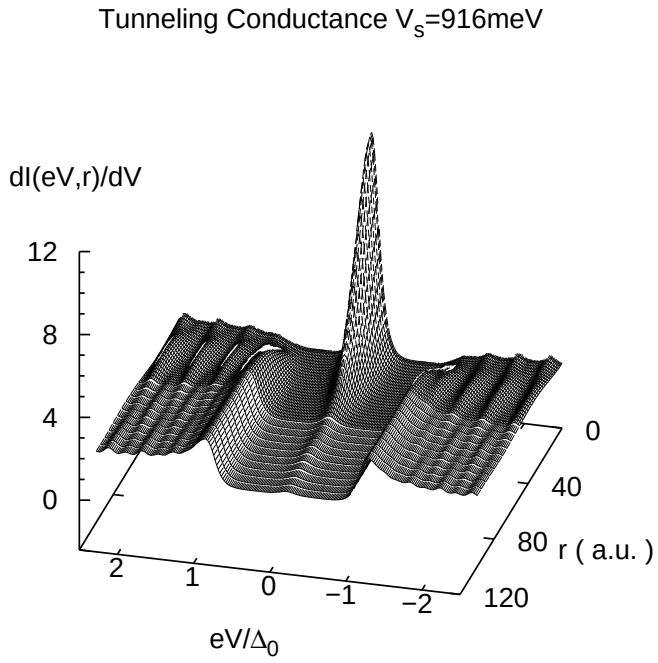

Figure 3.13: Tunneling conductance as a function of bias voltage and radial distance r for $V_s = 916$ meV.

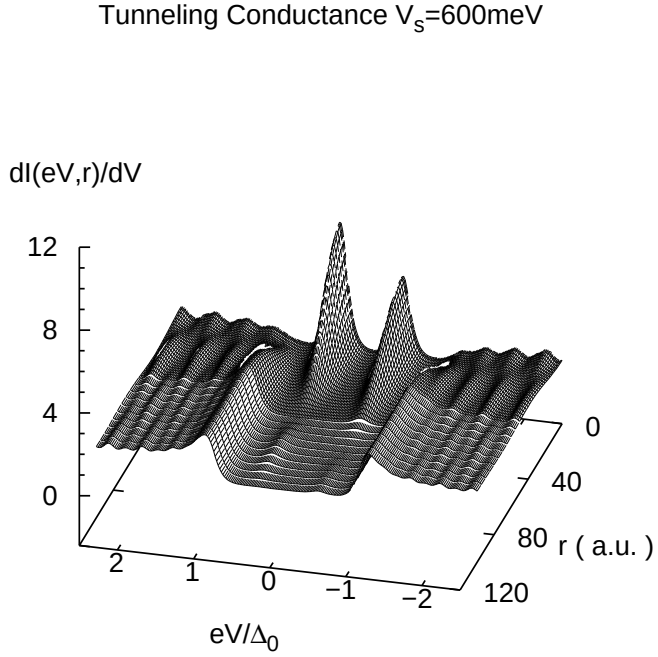

Figure 3.14: Same as Fig. 3.13 but for $V_s = 600$ meV.

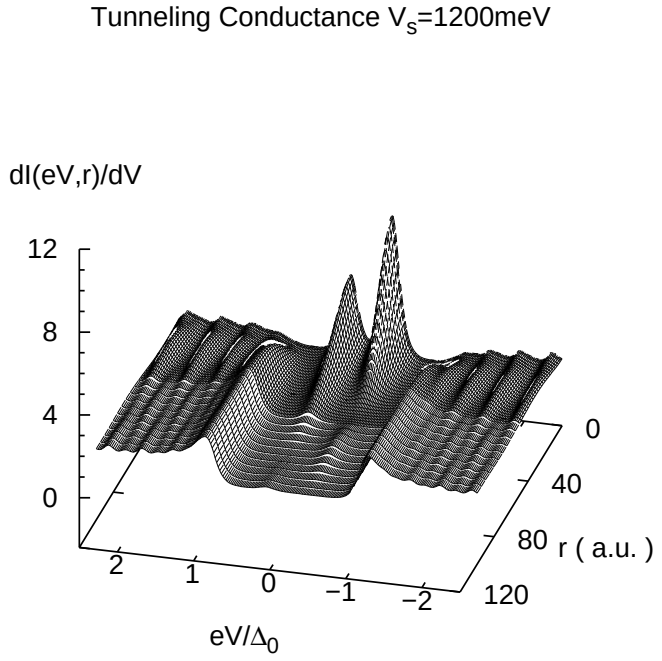

Figure 3.15: Same as Fig. 3.13 but for $V_s = 1200$ meV.

Chapter 4

Conclusion

4.1 Conclusion

In this thesis, to study inhomogeneous superconductivity around a single magnetic impurity, we have used the BdG theory of superconductivity including a magnetic interaction, and have developed program for solving the BdG equations selfconsistently, utilizing parallel computation. We have examined in detail the order parameter, quasiparticle excitation spectra, quasiparticle wavefunctions, and the local tunneling conductance.

In order to check the accuracy of the computational programming of the BdG equations, we have first studied the problem of a single magnetic vortex and solved the BdG equations for a two-dimensional superconductor, $NbSe_2$. The tunneling conductance around a vortex exhibits Andreev bound states of quasiparticles trapped in the "potential well" of the order parameter. This result is consistent with both experimental [11] and earlier theoretical [26] works.

We have then generalized our BdG equations to three-dimensional systems, and after reproducing the well-known BCS results for a homogeneous superconductor, we have investigated the effects of a single magnetic impurity by modeling the impurity by a classical spin and solving the spin-dependent BdG equations. The BdG equations were solved directly and numerically, until selfconsistency for the order parameter was obtained. Unlike the conventional BCS theory, which assumes translational invariance, selfconsistently solving the BdG equations has high numerical demand. Our study of inhomogeneous superconductivity has been made feasible by means of parallel computation on a large-scale Beowulf-class PC cluster here at the

University of Saskatchewan. Modeling Nb, the experimentally studied superconductor [20], is still not practical due to its very large Fermi energy, so we have performed our calculation for a model system similar to $NbSe_2$.

Similar to a vortex, a magnetic impurity tends to break up Cooper pairs and suppress superconductivity locally, trapping quasiparticles around it. A significant difference, however, from the vortex problem is that the magnetic impurity aligns the spin of the neighboring conduction electrons with its own. This results in particle-hole asymmetry in the local density of states and the tunneling conductance.

As the effective potential from the magnetic impurity has a very short range on the atomic scale, bound states exist for angular momentum $l = 0$ and 1 only, for a physically reasonable potential strength. We find two bound-state branches ($l = 0$), one for a spin-up quasiparticle (spin-up electron and spin-down hole) and another for a spin-down quasiparticle (spin-down electron and a spin-up hole). As the potential strength V increases from zero, the two bound states appear near the gap edge – with positive energy for spin-up quasiparticle and negative energy for spin-down quasiparticle – and as a function of V, their bound-state energies approach zero and cross at zero energy at a certain critical strength V_c. Beyond this critical strength, the two bound-state energies reverse their sign, and the nature of the quasiparticle bound states changes from that for $V < V_c$.

For $V < V_c$, the positive-energy bound state represents adding a quasiparticle excitation with spin up, and the negative-energy state corresponds to removing a quasiparticle with spin down. For $V > V_c$, however, the magnetic interaction with the impurity is so strong that, in the *ground* state, there is already a spin-up quasiparticle bound to the impurity. Thus the negative-energy excitation is the removal of this quasiparticle. On the other hand, the positive-energy state corresponds to adding a spin-down quasiparticle (spin-down electron or spin-up hole), which will form a Cooper pair with the bound spin-up quasiparticle and enter into the superconductor.

Our results for the tunneling conductance with particle-hole asymmetry are consistent with what has been observed experimentally [20]. In the experiment of Ref. [20], the tunneling conductance over a Mn atom and that over a Gd atom

showed opposite asymmetry. We propose that, within our model of a classical spin, this difference comes from a difference in the effective interaction between the magnetic atom and the conduction electrons in the case of Mn ($V > V_c$) and Gd ($V < V_c$).

References

[1] H. Kamerlingh Onnes. *Communications from Physics Laboratory at the University of Leiden*, page 119, 1911.

[2] W. Meissner and R. Ochsenfeld. *Naturwissenschaften*, 21:787, 1933.

[3] J. Bardeen, L. Cooper, and R. Schrieffer. *Physical Review*, 106:162, 1957.

[4] J. Bardeen, L. Cooper, and R. Schrieffer. *Physical Review*, 108:1175, 1957.

[5] J. Bardeen and R. Schrieffer. *Progress in Low Temperature Physics*, 3:170, 1961.

[6] J. Gavala. *Applied Physics Letters*, 23:480, 1978.

[7] J. Bednorz and K. Müller. *Zeitschrift für Physik B*, 64:189, 1986.

[8] A. Abrikosov. *Soviet Physics-Journal of Experimental and Theoretical Physics*, 5:1175, 1957.

[9] P. de Gennes. *Superconductivity of Metals and Alloys*. Boulder, CO: Westview Press, 1999.

[10] U. Essmann and H. Träuble. *Physics letters A*, 24:526, 1967.

[11] H. Hess, R. Robinson, R. Dynes, J. Valles, and J. Waszczak. *Physical Review Letters*, 62:214, 1989.

[12] H. Hess, R. Robinson, R. Dynes, J. Valles, and J. Waszczak. *Journal of Vacuum Science Technology*, A 8:450, 1990.

[13] C. Caroli, P. de Gennes, and J. Matricon. *Physics Letters*, 9:307, 1964.

[14] C. Caroli, P. de Gennes, and J. Matricon. *Physics Condense Matter*, 3:380, 1965.

[15] K. Tanaka, I. Robel, and B. Jankó. *Proceedings of the National Academy of Sciences of the United States of America*, 99:5233, 2002.

[16] P. Anderson. *Journal of Physics and Chemistry of Solids*, 11:26, 1959.

[17] K. Tanaka and F. Marsiglio. *Physical Review B*, 62:5345, 2000.

[18] A. Abrikosov and L. Gor'kov. *Soviet Physics-Journal of Experimental and Theoretical Physics*, 10:593, 1960.

[19] A. Abrikosov and L. Gor'kov. *Soviet Physics-Journal of Experimental and Theoretical Physics*, 12:1243, 1961.

[20] A. Yazdani, B. Jones, C. Lutz, M. Crommie, and D. Eigler. *Science*, 275:1767, 1997.

[21] L. Landau. *Soviet Physics-Journal of Experimental and Theoretical Physics*, 3:920, 1956.

[22] N. Bogoliubov. *Nuovo Cimento*, 7:794, 1958.

[23] J. Valatin. *Nuovo Cimento*, 7:843, 1958.

[24] J. Schrieffer. *Theory of Superconductivity*. CO:Westview Press, 1971.

[25] M. Cyrot and D. Pavuna. *Introduction to Superconductivity and High-T_C Materials*. World Scientific Publishing Co. Pte. Ltd., 1992.

[26] F. Gygi and M. Schlüter. *Physical Review B*, 43:7609, 1991.

[27] M. Tinkham. *Introduction to Superconductivity*. Doven Publication, Inc., second edition.

[28] B. Deaver and W. Fairbank. *Physical Review Letters*, 7:43, 1961.

[29] R. Doll and M. Näbauer. *Physical Review Letters*, 7:51, 1961.

[30] T. Smith and H. Rorschach. *Reviews of Modern Physics*, 36:277, 1964.

[31] V. Moshchalkov, L. Gielen, C. Strunk, R. Jonckheere, X. Qiu, C. VanHaesendonck, and Y. Bruynseraede. *Nature*, 373:319, 1995.

[32] K. Geim, V. Grigoreva, V. Dubonos, S. Lok, C. Maan, E. Filippov, and M. Peeters. *Nature*, 390:259, 1997.

[33] Y. Tanaka, A. Hasegawa, and H. Takayanagi. *Solid State Communications*, 85:321, 1993.

[34] M. Virtanen and M. Salomaa. *Physical Review B*, 60:14581, 1999.

[35] J. Sonier, R. Kiefl, J. Brewer, S. Dunsiger J. Chakhalian, W. MacFarlane, R. Miler, A. Wong, G. Luke, and J. Brill. *Physical Review Letters*, 79:1742, 1997.

[36] J. Fletcher, A. Carrington, P. Diener, P. Rodiére, J. Brison, R. Prozorov, T. Olheiser, and R. Giannetta. *Physical Review Letters*, 98:057003, 2007.

[37] P. Diener, P. Rodiére, J. Fletcher, A. Carrington, J. Brison, R. Prozorov, T. Olheiser, and R. Giannetta. *Phyica C*, 60:460, 2007.

[38] A. Andreev. *Soviet Physics-Journal of Experimental and Theoretical Physics*, 19:5, 1964.

[39] L. Kramer and W. Pesch. *Zeitschrift für Physik A Hadrons and Nuclei*, 269:59, 1974.

[40] A. Unsöld. *Annalen der Physik*, 82:355, 1927.

[41] S. Barnes. *Advances in Physics*, 30:801, 1981.

[42] J. Schrieffer and P. Wolff. *Physical Review*, 149:491, 1966.

[43] C. Kessler, M. Mehring, P. Castellaz, G. Borodi, C. Filip, A. Darabont, and L. Giurgiu. *Physica B:Condensed Matter*, 229:113, 1997.

[44] P. Joseph and P. Singh. *Solid State Communications*, 141:390, 2007.

[45] K. Baberschke. *Zeitschrift für Physik B*, 24:53, 1976.

[46] D. Morr and J. Yoon. *Physical Review B*, 73:224511, 2006.

[47] W. Press, B. Flannery, S. Teukolsky, and W. Vetterling. *Numerical Recipes in C: The Art of Scientific Computing*. Cambridge University Press, 2nd edition, 1992.

[48] M. Mori and R. Piessens. *Numerical Quadrature*. Elsevier Science Pub. Co., 1st edition, 1987.

[49] J. Mathews. *Numerical Methods for Mathematics, Science, and Engineering*. Englewood Cliffs, second edition, 1992.

Appendix A

Parallel Computation

Traditionally, a program runs on a single personal computer (PC) with a single CPU. Instructions are executed sequentially, and only one instruction can be executed at any moment. But in parallel computing, a program runs on more than one CPU at the same time. A problem is broken into different parts that are executed concurrently on different CPUs.

Because of constraints to building a PC with faster CPU and/or larger memory, it is believed that parallelism is the future of computing. Parallel computing on a pc cluster can save time, overcome memory constraints, and save costs by using multiple "cheap" PCs instead of a supercomputer. Parallel computation often makes numerical calculations for complex systems feasible.

A.1 Hardware

Our computation is performed on a Beowulf-class PC cluster, a 128-CPU 3GHZ Xeon cluster with Hyperthreading Technology, which allows one to use the cluster as having 256 CPUs. The PCs are connected via an extremely fast, low-latency network

There are mainly two kinds of memory architectures of a PC cluster, shared memory and distributed memory. The general characteristics of shared memory are that all processors have access to all memory as global address space (Fig. A.1). Different processors can operate independently but share the same memory resource, and changes in a memory location made by one processor are visible to all other processors. On the contrary, the distributed memory structure is that each processor has its own local memory (Fig. A.2). Fast interconnection among different CPUs are vital for data transfer on a large-scale cluster. The computer cluster used for our project has the distributed memory architecture.

A.2 Software

Message Passing Interface (MPI) is currently the most versatile model of parallel programming that is portable and most suitable for the distributed-memory architecture. It can be used even on a shared-memory machine. The MPI has been applied for the calculation presented in this thesis. The basic procedure of MPI is that the "master" process sends out input data to all the "slave" processes by Commands such as Send and Receive or Bcast (broadcasting), and each process then does its part of the calculation and sends (Send) the result back to the master node (Receive). In this last procedure of data collection, for example, calculation such

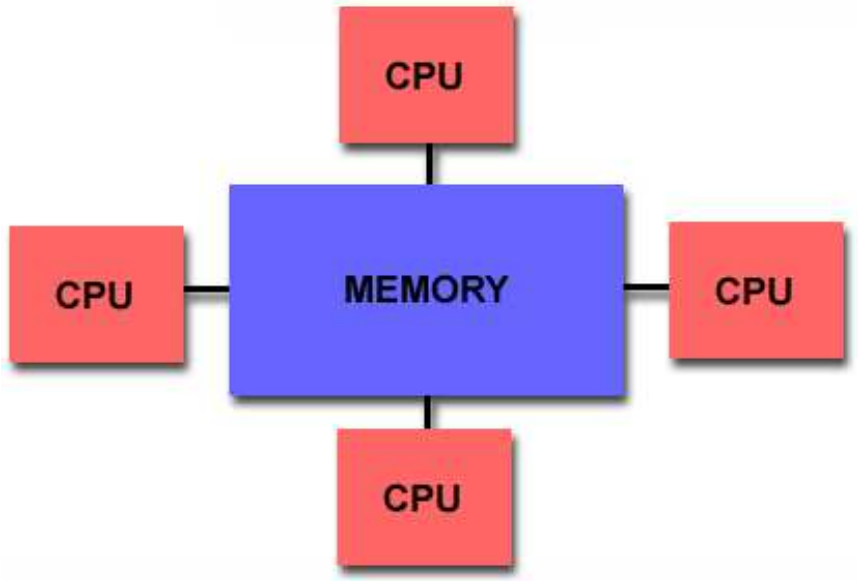

Figure A.1: A shared memory architecture

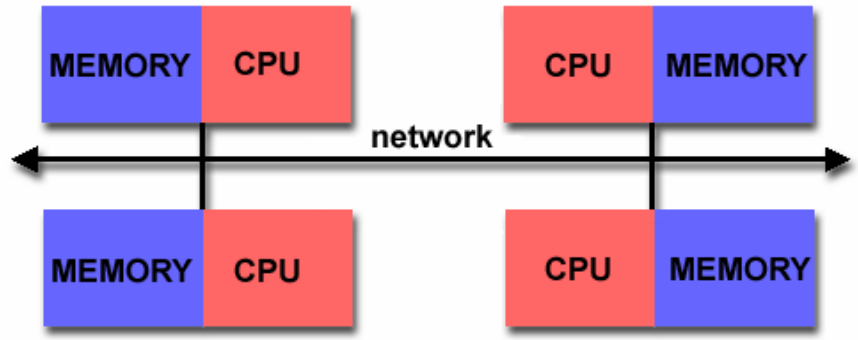

Figure A.2: A distributed memory architecture

as summation (Reduce) can be made on the master process and sent to the slave processes by Bcast. These two procedures can also be performed in one step by Allgather (Allreduce for summation), by which the data are collected on each process.

MPI is most effective for "coarse-grained" parallelism, where most of the computational time is spent on independent calculation in each process and the amount of data communication as described above is minimal. This is the case for our selfconsistent calculation. Selfconsistent iteration, where each iteration step needs results from the the previous iteration, cannot be parallelized. However, within each iteration, calculations for different values of angular momentum l are independent and can be performed on different processes. In this procedure, the input order parameter is broadcasted, and each process diagonalizes the matrix in Eq. (2.8) and calculates the partial contributions to the order parameter in Eq. (2.11) for a set of l values. Then all the contributions are collected by the master process to calculate the new order parameter, and convergency is checked. If not converged to the desired accuracy, it

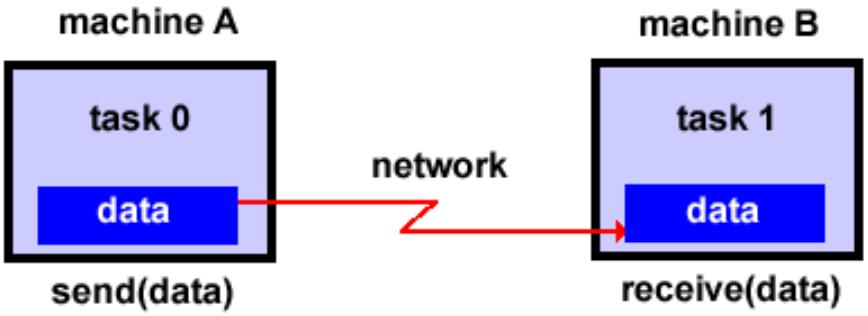

Figure A.3: Message Passing Interface model

initiates the next iteration. A flow chart of this procedure is shown in Fig. A.4.

The order parameter is calculated at discretized positions $\{r_i; i = 1, ..., N\}$. The convergence is checked by summing the local error, $\Delta_{\text{new}}(r_i) - \Delta_{\text{old}}(r_i)$, over i and dividing the sum by N. We require that the average error is smaller than 10^{-4}. Double precision is used for all the calculations presented in this thesis, and the Bessel functions are expected to be accurate to 10^{-16}.

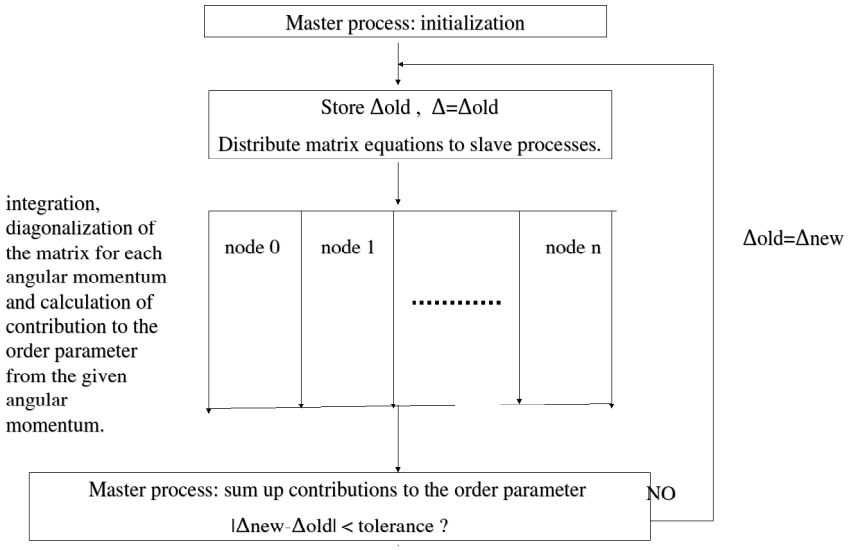

Figure A.4: Flow Chart of the Computation

A.3 Computation

A.3.1 Homogeneous System in Two Dimensions

For a homogeneous system in two dimensions, the submatrices T and $\widetilde{\Delta}$ are both diagonal as shown in Eqs. (2.9, 2.10), and those diagonal elements are easy to obtain. This real, symmetric matrix is reduced to a tridiagonal form by Householder reduction [47] and the reduced matrix is solved by QL algorithm [47].

A.3.2 Isolated Vortex Problem

The calculation procedure of the vortex problem is basically the same as that of the homogeneous model as shown in Fig. A.4. However, the pairing potential is now a function of position and the submatrix $\widetilde{\Delta}$ is no longer diagonal (Eq. (2.28)). The evaluation of the matrix elements is time-consuming and the calculation is coarse-grained. The integration is difficult due to strong oscillations of the Bessel function, especially when the nodal quantum number is large. Several integration algorithms were tried, including routines trapzd, qtrap, qsimp, qromb and qgaus from Numerical Recipes in C [47]. The Fortran routine QAG of the integration package QUADPACK from Netlib, which can deal well with a strongly oscillating integrand, has turned to be most reliable [48].

The pairing potential $\Delta(r)$ at the end of each iteration is evaluated at a set of discrete positions. To calculate the matrix elements for the next iteration, curve fitting is needed to evaluate $\Delta(r)$ at any r required by the integration routine. Interpolation and extrapolation are common choices of curve fitting. However, QUADPACK requires the integrand to be a smooth function. To guarantee smoothness, another kind of curve fitting, the trigonometric polynomial method, is used to construct a smooth function to best fit the discrete data of $\Delta(r)$. This method is discussed in details in Appendix B.

A.3.3 Homogeneous System in Three Dimensions

The programs are similar to those for solving the homogeneous problem in two dimensions, except that numerically evaluating the spherical Bessel functions is more difficult than the Bessel functions of integer order near the origin. This had to be taken care of when performing the integrals for the matrix elements.

A.3.4 Isolated Magnetic Impurity Problem

The numerical evaluation of the matrix elements of $\widetilde{\Delta}$ is more difficult than that in the vortex problem. This is due to the fact that integrating the spherical Bessel functions costs much more time than integrating the Bessel functions of integer order. To reduce the computation time, the matrix elements were evaluated in two regions separately. Since the range of the impurity potential (10 a.u.) is so much smaller than the system size (R =8000 a.u.), it can be assumed safely that the order parameter

is constant in the region $[0.3R{:}R]$. Thus we store the values of the integral in this region, and perform the integration only in the region $[0{:}0.3R]$ at each iteration. The two parts are combined to yield the matrix elements of $\widetilde{\Delta}$.

Appendix B

Curve Fitting

The trigonometric polynomial method [49] is used to make curve fitting of the discrete data of the pairing potential. The basic idea of this method is presented in the first section and its application to our calculation is explained in the second section.

B.1 Trigonometric Polynomial Approximation

A trigonometric polynomial of order M can be written as

$$T_M(x) = \frac{a_0}{2} + \sum_{j=1}^{M}(a_j \cos(jx\pi) + b_j \sin(jx\pi)). \tag{B.1}$$

When the parameters, a_j and b_j, are chosen properly, the polynomial $T_M(x)$ can fit a discrete function $\{f(x_k) : x_k\}$.

Assume that $f(x)$ is periodic with period 2π and there are $N+1$ points with equally spaced abscissas in the region $[-1, 1]$:

$$x_k = -1 + \frac{2k}{N}\,, \tag{B.2}$$

where $k = 0, 1, \cdots, N$ and N is an integer. An approximate function $T_M(x)$ $(2M + 1 \leq N)$ is determined by minimizing the quantity

$$\sum_{k=0}^{N}(f(x_k) - T_M(x_k))^2\,. \tag{B.3}$$

The coefficients a_j and b_j of the polynomial are

$$\begin{aligned} a_j &= \frac{2}{N}\sum_{k=1}^{N} f(x_k)\cos(jx_k) \quad j = 0, 1, \cdots, M, \\ b_j &= \frac{2}{N}\sum_{k=1}^{N} f(x_k)\sin(jx_k) \quad j = 1, 2, \cdots, M. \end{aligned} \tag{B.4}$$

B.2 Fitting the Pairing Potential

The order parameter $\Delta(r)$ is evaluated at a discrete set of points by solving the BdG equations. For the next iteration, it is needed as a smooth function of r. To

apply the trigonometric polynomial approximation, $\Delta(r)$ is extended for normalized coordinate r from region [0:1] to region [-1:1]. For the vortex problem, as the order parameter goes to zero linearly as $r \rightarrow 0$, it is assumed to be an odd function, $\Delta(-r) = \Delta(r)$. For the impurity problem, it is assumed to be an even function.

The trigonometric polynomial T_M is an approximation whose precision depends on the choice of the parameter M. The larger the M, the closer the approximation to the original function, but the upper limit is set by $2M + 1 \leq N$. In our calculation, $N \approx 3000$. After comparing the curve fitting with different orders M, we believe that a reasonable approximation can be obtained for the order parameter for $M = 150$.